POLITECNICO DI MILANO

Master of Science in Material Engineering and Nanotechnology

School of Industrial and Information Engineering

POLITECNICO
MILANO 1863

REFRACTORY METAL COATINGS ONTO CARBON MATERIALS FOR PLASMA FACING COMPONENTS

Supervisor: Prof. Massimiliano Bestetti

Master Thesis by

Mehmet Cemal Atay

ID: 913400

Academic Year 2019 – 2020

TABLE OF CONTENTS

LIST OF FIGURES

ABSTRACT

The paper gives information about material selection and fabrication methods for producing Plasma Facing Components (PFC), which are used in the walls of nuclear reactors. Refractory metals were chosen as coatings and, graphite was selected as a substrate. The thermomechanical and structural properties of the layers were discussed. Furthermore, production methods of these coatings are evaluated to estimate the optimum way based on the experiments in this literature. Finally, a comparison between these fabricated coatings was discussed by assessing both structural deteriorations and thermomechanical properties during their application processes. Particular attention is paid to PVD fabricated tungsten coatings over graphite due to its overwhelming performance acting as PFC.

1. INTRODUCTION

Nuclear fusion science has become popular since the 1950s due to its safe, cleanness, and availability at large scales. The development of nuclear fusion reactors to get the best efficiency continued until today. Further investigations are related to the International Thermonuclear Experimental Reactor in which the main achievement is to be operating at high efficiencies, getting ten per one net energy. However, achieving these goals are highly related to material selections and their availabilities. The key issue in fusion reactors due to the hazardous environment of nuclear fusion reactors is the right material choices. It is found out that fifty percent of the problems in obtaining the best efficiency is related to material selections and their limiting properties.[1][15]

1.1. Plasma Facing Components

The plasma-facing components at first wall applications have an essential role in the performance of the system due to exposure to severe operating conditions. These requirements will induce superior material selection and design to PFC technology. Since the desired properties of the PFCs depend on the operating conditions, having an idea about these conditions is also essential. At the first wall of tokamaks, the PFCs are expected to be load with a neutron load of 1 MW/m, surface heat flux of 0.6 MW/m, disruptions with 2 MJ/m, and run-away electrons with 300 MeV which have an energy density of 30MJ/m. Water can be used as a coolant due to its operations with passive safety. By the time coverage of the first walls have been done by low Z materials to provide necessary protection against disruptions, neutral beams. Also, to minimize the flow of high Z impurity.[18] The main difficulty is to control and limit the flux of contaminants into core plasma. This requires the right choice of materials as a plasma-facing component. The early usage of high-Z materials, plasma facing components were led to undesired results due to the core contaminations. Besides, the low-Z materials used a plasma-facing component, which is mainly based on carbon were used in the various tokamaks. *[3]* Among the different types of low Z materials, carbon-based ones were studied because of their brilliant thermal shock resistance. Carbon fiber composites are good candidates for reference materials due to their excellent tailorable aspects for specific applications.[18]

The main drawback of carbon is those own weaknesses which are chemical and physical sputtering yields. Carbon also suffers from different mechanisms than sputter yield at high temperatures. For example, High-Density graphite, which performs with a minimum oxidizing

issue as structural material still suffers from oxidation and oxidation related erosion above 1000°C. This drawback of graphite limits its usability for high temperatures and extreme conditions. Because of this limitation of graphite, providing a ceramic coating layer is necessary for determining the oxidation of graphite and be able to perform without drawbacks, which increases its lifetime at high-temperature operating conditions. Conventional ceramic coatings like silicon carbide (SiC), silicon nitride (Si_3N_4), and molybdenum disilicide ($MoSi_2$) exhibit good aspects to prevent the oxidation process. However, their capability for oxidation resistance cannot exceed 1800 °C for many cases, for the most general case, SiC ceramic coatings could resist oxidation below 1650 °C. Besides, after 1800 °C SiC oxidize in a fast manner. Replacement of the conventional ceramic coatings for high-temperature applications can be achieved via using early transition metals of Group IV and V. Such as tantalum, titanium, zirconium, and Molybdenum. These refractory metals have high melting temperatures and form stable oxides. [2]

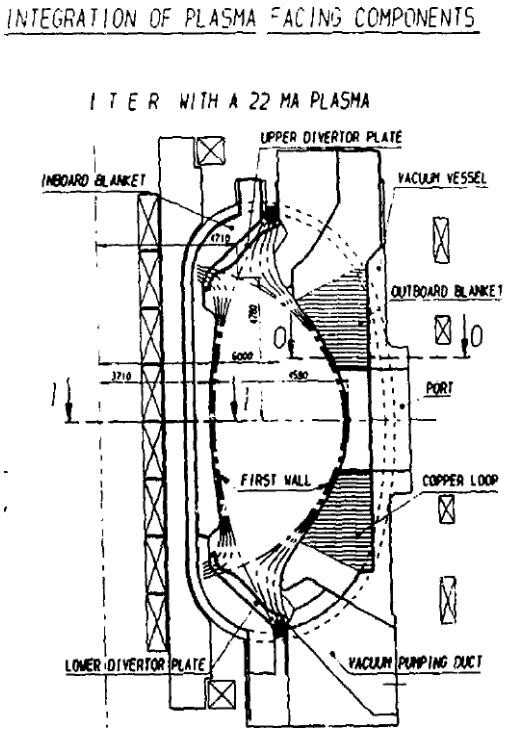

Figure 1 - Integration of the Plasma Facing Component) [18]

1.1.1. Refractory Metals – Carbon Substrate Plasma Facing Components

Tungsten

Refractory metals are studied to be used as a part of PFCs due to their high thermal and plasma erosion resistance. Particularly, tungsten (W) gets the most attention. It has a fine grain structure and manageable ductility via alloying. Also, it exhibits moderate tritium retention.[19] With many desired properties tungsten has high melting temperature, low vapor pressure, good thermal conductivity, high-temperature resistance, stability, and a high threshold for sputtering. There is no hydride formation or co-depositing with tritium.

One drawback of tungsten is, it has a high atomic number which may lead to impurities in plasma. [15] But due to its high atomic number Z, it exhibits lower sputtering yields which are critical for the wear and the erosion of First Wall applications at high temperatures. Materials at the First Wall will operate at the temperature range of 800 K – 3500 K with a mean power density of 8MW/m^2 in which the erosion will be induced due to hydrogen and impurities. By the erosion, sputtered particles will change the plasma behavior. As a result, plasma-wall interactions will be significant for material selection.[17] Due to low yield sputtering under the bombardment of hydrogen with prompt redeposition combined with good thermal properties, tungsten became a great candidate for PFC at nuclear fusion first walls.[12] It requires high energy to exhibit sputtering by hydrogen with having low effective yield sputtering. Compared to low Z materials like carbon, sputtered atoms from tungsten will have tendencies to display prompt redeposition at high electron densities due to short ionization lengths, and large gyroradius. Also, the thermomechanical properties of the tungsten are quite preferable. tungsten exhibits high thermal conductivity even at very high target temperatures [>100 W/m-K at 1500°C]. Relatively high mechanical strength by having the highest melting point and the lowest vapor pressure among other metals.[4]

As mentioned above, tungsten (W) has excellent thermal properties, the highest melting point of approximately 3410 °C, a great thermal conductivity of 173 W m−1 K, a high sputtering threshold with low tritium retention.[22] However, due to its high atomic number, the maximum tolerable concentration of sputtered tungsten is much lower than the low Z elements.[14]. Also, bulky tungsten is hard to machine because it is already brittle at room temperature. Depending on the impurities, deformation histories, and grain size, ductile – to – brittle transition

temperature of the tungsten is between 150°C – 400 °C. The recrystallization process starts at 1150°C, which leads to a reduction of mechanical strength. This reduction in mechanical strength may lead to material failure due to thermal fatigue.[4] Also, due to extreme operating conditions in the fusion reactor, tungsten may exhibit embrittlement as a result of particle bombarding or thermal shock loading.[22] Besides, high Z materials will cause high radiative power losses.

Bulky tungsten will have high electrical conductivity which leads to substantial eddy currents activated by high energy neutrons.[20] To overcome these problems, instead of bulky tungsten, thin layers must be used to form a composite. Studies to coat tungsten over graphite are ongoing for 15 years. The purpose is to combine the superior effects of two materials to obtain a composite that is fit for first wall applications. Different VPS, PVD, and CVD techniques were advanced to coat W over carbon-based materials as the first wall application at fusion devices. Testing of the coating which comes from different methods was done by performing other thermal loads. Beams of electron or ion are also simultaneously applied to simulate fusion plasma conditions. The results of laboratory W coating experiments are consistent with industrial approaches. CMSII technology applied to the industry for the W coating of tiles including divertor tiles for the ITER-like Wall project at JET and ASDEX Upgrade. The thickness of the coatings is changing between the range of 10- 15μm or 20- 25μm. Tile position is the dominating aspect of the thickness of the coating. Besides, a coating that has a thickness of ~50μm was fabricated and tested in GLADIS up to 23MW/m^2. *[13]*

However, since there is not any additional carbon diffusion barrier considered between graphite and tungsten, these technological coating advancements require proof that the thermal stability of tungsten over the carbon-rich substrate, like graphite. As a result of carbon diffusion through tungsten, the tungsten carbides may be formed by precipitation and its thermo-mechanical properties must be necessarily evaluated. *[1]*

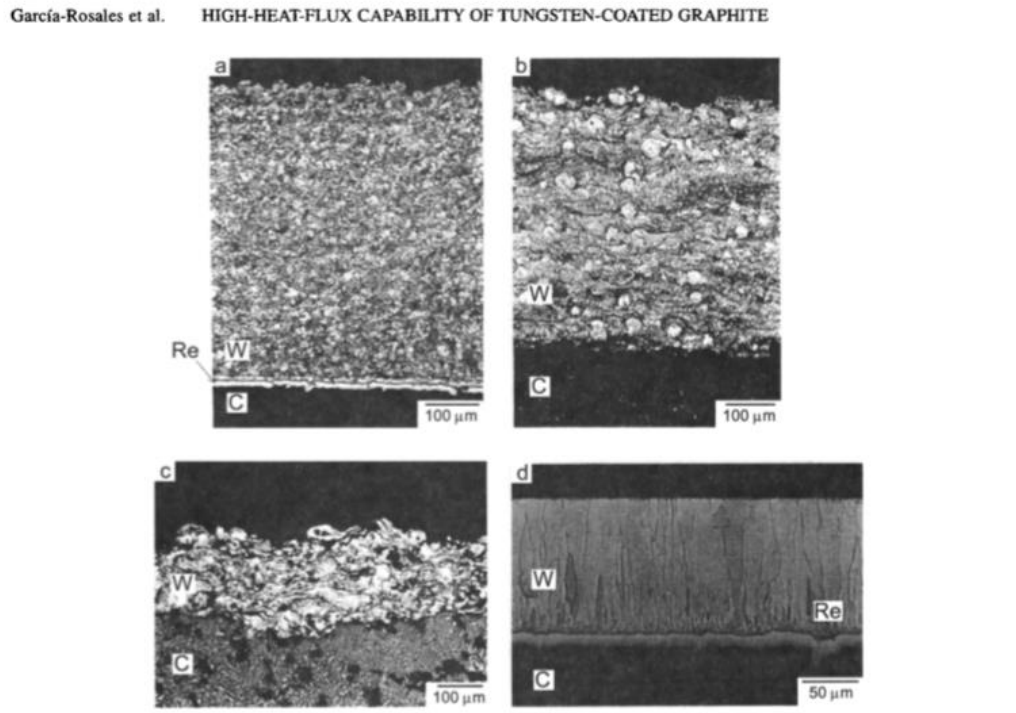

Fig. 2. Sections of different tungsten coatings on graphite: (a) VPS coating from PI/SM with rhenium-containing intermediate layer, (b) VPS coating from Forschungszentrum Jülich, (c) IPS coating from CEN, and (d) PVD coating from Plansee AG with rhenium-containing intermediate layer.

Figure 2 - Sections of different tungsten coatings on graphite [4]

Tantalum Carbide:

Tantalum carbide (TaC) is a promising ultra-high temperature ceramic (UHTC) material to coat necessary surfaces, which is adopted in applications such as rocket nozzles, aerospace propulsion systems, brake lines, and high-performance cutting tools. Tantalum has an extremely high melting temperature of 3800 °C, relatively high hardness (20 GPa), outstanding oxidation and thermal shock resistance, and excellent ablation resistance. [2] However, CO and CO_2 gaseous are unavoidably occurred because of the oxidation process. Oxidation leads to porous oxide scales that could delaminate and peel off. The most common oxide type of tantalum carbide is Ta_2O_5, with a melting point of about 1900 ◦C, which is a low temperature to perform as a plasma-facing component. In conclusion, the oxidation of tantalum carbide would lead to melt and lose its structural integrity, which eventually leads to failure. Reducing the oxidation process is crucial to have TaCs as a plasma-facing component. [5]

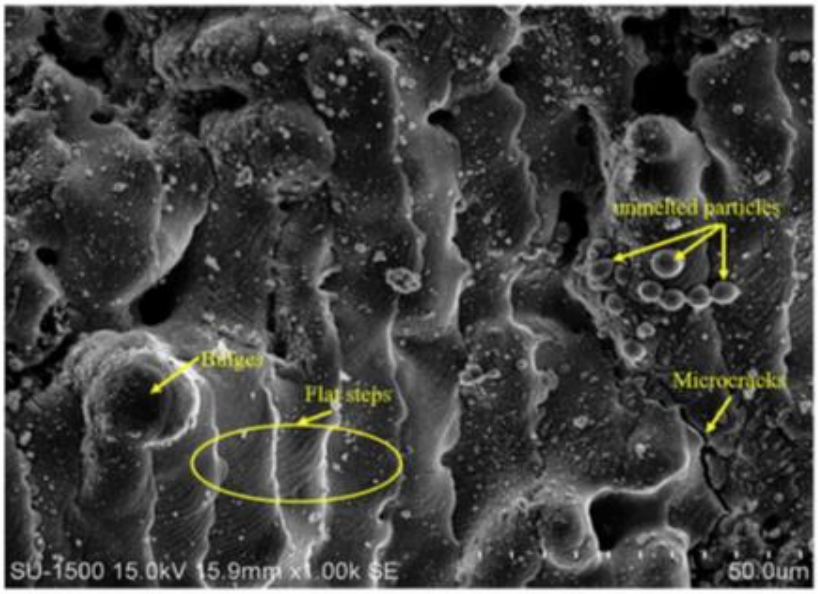

Figure 3 - Microstructure of TaC coating [2]

Molybdenum

Molybdenum has one of the highest melting temperatures among other metals with having density exceeding the iron by 25%, which is lower than other high melting point metals. Also, it exhibits a meager thermal expansion under high temperatures compared to other engineering materials. Besides, Molybdenum has a thermal conductivity that exceeds most of the elements in the periodic table. Even though Molybdenum has high thermal properties, its relatively low density still adversely affects thermal stability. Also, it will be heavy and will require extra structural supports at the final design. Toward solving this problem, molybdenum-graphite composites were investigated in the mid-late 1900s for high-temperature applications like aerospace and nuclear reactors. [6]

Nonetheless, molybdenum-graphite composite exhibited a relatively brittle character, thus led to low mechanical strength. Further tests were carried over laboratory with small-scale specimens, and no significant developments occurred ever since. By having an excellent plasma-facing component, the requirement of a new composite material, which could eliminate the disadvantages of the previous ones and withstand demanding conditions. Possible composite material, which is related to the present invention, consists of molybdenum carbide,

graphite, and carbon fibers. The researches have shown that forming molybdenum carbide - carbon composite including carbon fibers enables one to combine the favored aspects of metals (high electrical conductivity and high fracture toughness) with high thermal conductivity, low density, and a low coefficient of thermal expansion. This mixture of properties allows the new composite materials ideally for high thermal performance applications like plasma-facing components at nuclear fusion reactors. [6]

This development requires the understanding of forming molybdenum carbide over carbon-based structures like graphite. Limited information about the wetting of graphite by liquid metals is available. Munson determined the surface energies of some liquid metal interactions at interfaces with carbon are determined by classical wetting theory applied to some non-reactive liquid metal-graphite systems by Bushmer and Heintz. High-temperature diffusion can be considered as another aspect of carbon-metal interactions between carbon and metallic materials. Carbon is a relatively small atom that can scurry within metal and carbide lattices by interstitial vacancies. However, vice versa, the diffusion of metal atoms through graphitic materials is less favorable, challenging, and slower due to the big atomic size of metals. [7]

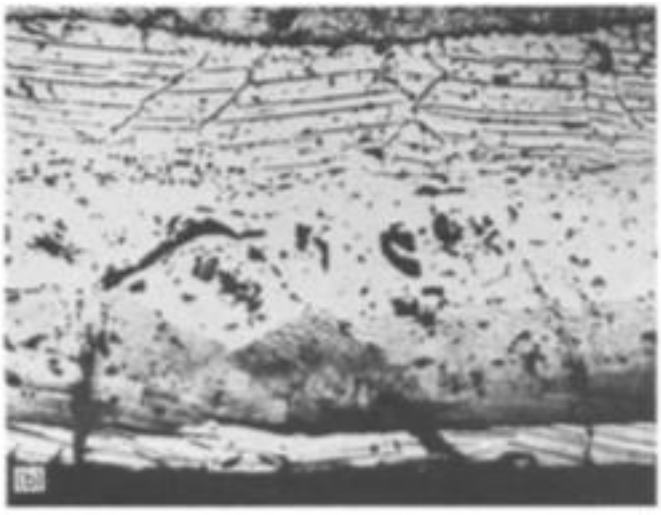

Figure 4 - Molybdenum Pyro-carbon diffusions [7]

Estimation of carbon diffusion in carbides can be done via the layer growth technique. Metallographic techniques allow us to measure the growth of different carbide layers during the reaction of carbide forming metals with carbon at very high temperatures. Since interfaces

exhibit a parabolic rate of growth, thus the application of classical kinetics with the theory of carbon diffusion coefficient can be determined for each carbide layer. However, this method is applicable under certain assumptions; layer growth happens only by diffusion, no metal diffusion through carbon is allowed, and the ability to diffuse must not depend on the variations of compositions within layers. This technique was used to determine the distribution of carbon through tantalum and columbium carbide. [7]

The orientation of the graphite affects the interfacial interactions between graphite and Molybdenum, which are systematically found by diffusion, wetting, and binding experiments. Since free bonds are accessible at peripheral carbon atoms and the ease with which they may remove the interactions are faster through parallel direction with graphite sheets. Merging of the graphite sheets in the graphite with the carbon sublattice in the Mo_2C lattice is determines how strong is the attachment between graphite edges and carbide products. It has been acknowledged that molybdenum carbide, which is promoted by hot working exhibits a fine dispersion that is adequate for bonding with graphite flakes in the composite material. This property inhibits the minimum slip and fracture at room temperatures. As a result, a tremendous increase in the mechanical strength of the graphite matrix is observed. Specimens can be molded between graphite dies due to the plasticity of Mo_2C above 1800◦C is appropriate for the molding process. The mechanism of wetting, bonding, dissolution, and precipitation have shown that all molybdenum graphite systems may require possible combination techniques for all graphite bodies. *[7]*

1.2. Coating Techniques

1.2.1. Physical Vapor Deposition

Different kinds of deposition techniques of thin films are covered by the Physical Vapor Deposition (PVD) technique. Some of the examples are evaporation, laser ablation-deposition, vacuum-arc based deposition, and magnetron sputtering. Small clusters of atoms or atoms which are not in the gas phase generally involved in the PVD. These particles are ejected to vacuum from a liquid or a solid source. Then they are transferred to medium and deposited over a solid to form a thin film. Removal of the particles or atoms from the source occurs via thermal heating of the source or bombarding the source with energetic particles like electrons, ions, molecules, or photons. This eject process is called sputtering. Also, the removal process could

be thermodynamical; evaporation occurs near the surface, which results in the kinetic ejection of particles. After ejection particles are diffuse into the vacuum chamber until they arrive on the solid substrate and condensate to form thin films.[23]

In general, chemical reactions occur at chemical vapor deposition. (CVD) Because the source is a gas as oppose to PVD in which the source can be liquid or solid that has very low vapor pressure. However, chemical reactions can occur in PVD systems on the thin film surface. Or a reactive gas species can be induced to the system to promote oxidation of thin film. This feature will necessarily alter the sources in PVD too.[23]

There are many different types of sources in the PVD process. The boat source is founded by a refractory metal (W-Ta). It is heated by passing a large current from the metal boat. The crucible source is made from a ceramic cup and surrounded by metal wires which are resistively heated. The electron beam source is the most commonly used one based on using a high energy electron beam that is ejected from a filament and projected over the source. By using an electron beam as a source, the risk of having any contamination is also decreased. Because in the electron beam source, only the target surface is heated in the other types of sources, boat and crucibles are heated, which may lead to eject of undesired particles into the system. The projectile of the emitted electrons is determined by applying a magnetic field.[23]

Plasma sources can also be used in PVD to provide sputtering via ion bombardment. Plasma can be generated by applying an electric field into an inert gas medium. High energetic electrons will generate ions by making collisions, and the ions will bombard the target to sputter atoms and atom clusters. This process can be done with higher efficiency by using magnetrons which form a magnetic field in the region near the cathode with a pressure of 0.5 – 30 mTorr. Above these pressures, the magnetron sputtering continues. However, the efficiency becomes negligible because of the many collisions occurring in the system between the gas and the sputtered atoms. This field controls the pathways of the electrons, leading them to circle magnetic field lines. As a result, their path length increase. Due to the hollow cathode effect localization of the electrons will increase the plasma density also the sputtering processes. Operation of the magnetron cathode occurs at very high discharge currents, and current densities can be achieved at discharge voltages of a few hundred volts. Magnetrons can operate as nearly ideal diodes. As a result, the increase of the discharge current can be almost indefinitely. This process will continue to occur until the current limit of the power supply is reached, or the target melts. [23]

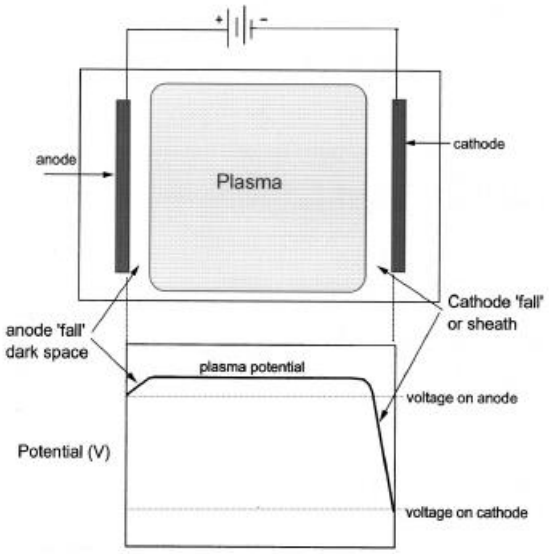

Figure 5 - Sketch of simple diode plasma [23]

1.2.2. Plasma Spraying

In the plasma spraying process, metallic and non-metallic particles are deposited over a substrate in a molten or semi-molten state. The thermal spraying process occurs at atmospheric pressure, and the heat source can pass 8000K to be able to melt any kind of material. It is preferable that to have excellent deposition efficiency melting temperature should be less than 300K of vaporization or decomposition temperature. The type of source can be direct current or radio frequency discharge. Particles are ejected to plasma at radio frequency discharges or to plasma jets in direct currents in which the clusters are accelerated and deposited over the substrate to form lamellae or splats. Thin films occur through the accumulation of these clusters. [24]

In the industry, thermal plasma spraying is preferred to fabricate high-added-value coatings due to its cost-efficient processing. Plasma spraying is done over the substrate to improve its heat, erosion, corrosion, and wear resistance. Also, surface aspects of the substrate can be altered via plasma spraying; it can restore the damaged surfaces of the composites, ceramics, and refractory metals. [24]

Accumulated clusters will exhibit a variety of microstructures at different length-scales. Also, it is expected to have vacancies, voids, and microcracks at the thin film. These defects may occur due to the high deposition rate at a relatively less controlled system in which the deposition rate is very high compared to the PVD process. Also, it is expected to have oxidation products as a drawback of this operation at the atmospheric pressures. Sub-systems can control film properties deposited by plasma spray; the plasma formation and its interactions, injection of particles from the powder (temperature, velocity, diameter, etc.), and the formation of the coating. [24]

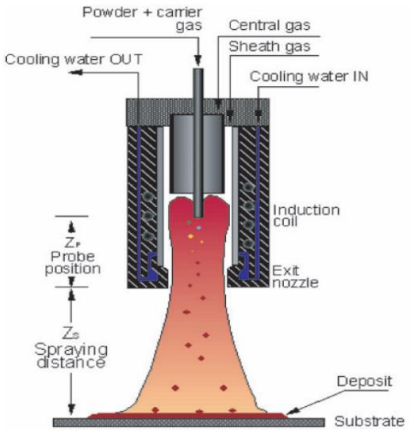

Figure 6 - Plasma Spraying – RF torch [24]

1.2.3. Chemical Vapor Deposition

Chemical vapor deposition (CVD) can be used to produce powders and pure bulk materials, but generally, it is used to fabricate solid thin film coatings to cover surfaces. A broad range of materials could be deposited as thin films with the CVD process. In the CVD method, a gas chamber that contains the heated substrate is used. The coating material is injected into the system via flowing precursors. At the surface of the hot substrate, chemical reactions take place, which results in a deposition of the thin film over the substrate. By-products of this chemical reaction are forced out from the gas chamber with an exhaust system. A variety of materials can be coated with different CVD setups. The wall could be hot or cold, and pressure can range from sub-torr to atmospheric pressure, and a temperature that varies 200°C – 1600°C. Also, plasmas, ions, photons, lasers, or hot filaments may involve improving the CVD process. [25]

CVD technique has many advantages to fabricate thin films. PVD process which depending on the sputtering or evaporation requires a clean line of sight that significantly affects the conformal coverage of the thin film and the thickness uniformity. But CVD processes display very high conformal coverages. The thin films have very close thicknesses along the covered surface even if the surface is not flat. Also, insides, undersides, and holes can be covered. Besides, complex shapes can be coated by the CVD technique. Because in CVD, chemical reactions take place at the surfaces that the coverage does not depend on the line of sight. Also, in CVD very high purities can be achieved with high deposition rates by having an efficient exhaust system in which the vacuum is not as high as PVD. [25]

CVD also displays some disadvantages. Precursors must be volatile at room temperatures. And the PVD process can exhibit very toxic aspects due to having chemical reactions. This drawback will restrict the number of precursors that can be used in the CVD process. [25]

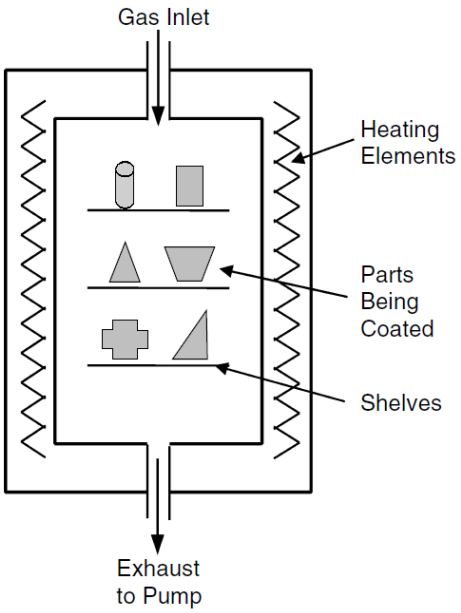

Figure 7 - Schematic drawing of hot-wall CVD reactor [25]

1.3. Adhesion Characteristics of the Thin Films

Adhesion between the thin film and the substrate is the key element to determine the performance of the composite material as a plasma facing component. Besides, the properties of the adhesive forces should not be altered dramatically by severe operating conditions. Through obtaining a good adhesion between coating and substrate certain mechanisms must be understood. The coatings are designed to endure specific and extreme conditions or to satisfy the required properties. Coating types can differ from metallic to ceramic and organic or composite materials. Substrates could be metallic but in general, they are non-metallic. In the coating systems since the substrate and coating are composed of different classes of materials, thus they exhibit different lattice and microstructures. As a result, they show very different properties. Also, severe operation conditions will apply relatively high stress to this coating – substrate interface. Adhesion between coating and substrate must be enough to bear these loads to endure operation conditions. However, obtaining this adhesion is not easy due to the involvement of different kinds of materials. Considering this situation, the mechanism of adhesion can be divided into three simple groups; mechanical interlocking, physical bonding, and chemical bonding. [8] The bonding that formed to connect the substrate and the coating may break down due to different reasons. The main reasons for this failure can relate to tensile (perpendicular to the interface) and shear stress (along the plane of contact). The coating can constrain rigidity higher than the substrate, which leads to fracture within the substrate. Whereas adhesion at the interface exceeds the cohesion of the substrate the cohesive failing will occur.

1 μm – 2 μm thickness of tungsten coatings was decently grown on the graphite. However, the W coatings with a thickness of 5 μm – 7 μm exhibited a lack of adhesion on the graphite substrate. It is acknowledged that tungsten coatings over carbon substrate experiencing low-intensity ion irradiation the adhesion-related failure happens due to the weak bond formation at the interface, in the case of high-intensity ion irradiation the adhesive failure happens due to cohesive failure at the carbon substrate. [17]

When the strong chemical bonding is not formed due to the different type of substrate - coating combination for example in the case in polymer coatings on metals, thermal spraying coatings or complete mismatch of materials as in the CFRP mechanical interlocking is the best mechanism to sustain necessary adhesive strength between substrate and coating. Size and

geometry at the locking sites are responsible for the transmission of the forces. These sites can form by different aspects like mechanically machined dovetails, grooves, and other macroscopic shapes and micro-roughness produced by grit blasting. With relation to surface properties of the substrate, three different effects can be considered, increase in surface area which will lead to different physical or chemical bonding to be more effective, friction force will take place between coating and substrate material and this frictional force will be high due to high friction coefficient and high normal stresses which can be occurred by coating shrinking on the substrate due to high operating temperature and high expansion coefficient of the coating material. [8] In general, it is known that the main adhesion aspects of the thermal spray deposited coatings are mechanical interlocking. Thus, at the interlocking sites, which are produced by the grit blasting process, there may not be enough adhesion forces that occur. This happens specifically if coupled materials exhibit different crystal structures. [15]

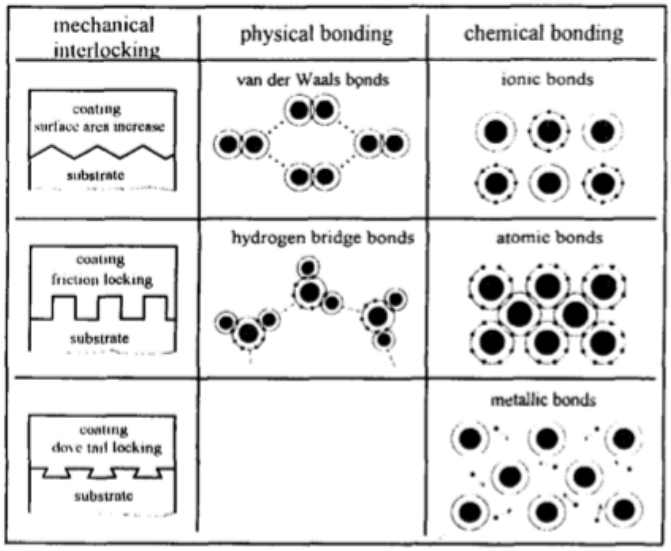

Figure 8 - Schematic diagram of different bonding mechanisms [8]

1.4. Thin Film Internal Stresses

Internal stresses in thin films can be estimated with the help of the ideal direction method. In this method, internal stress at the coatings are related to texture shape and the interaction between the crystals. Each of these stresses can be linked to different textures of the thin film.

XRD can be used to analyze thin films by having a diffractometer and a goniometer. The idea for the ideal orientation method is based on the measurement of the lattice strains. A sufficient amount of diffraction intensity can be obtained direction of the measurement must concerning the texture. Evaluated strains can be related to internal stresses in the texture by knowing the elastic constants. For example, in the molybdenum thin film case determining the internal stresses of textured by ideal direction method by evaluating texture shape and crystal interactions. It demonstrated that internal stresses in PVD molybdenum films are very high compressive stresses. [9]

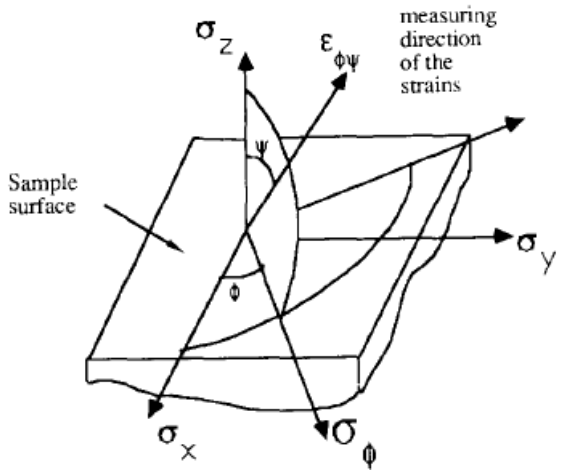

Figure 9 - Coordinate system for X-ray internal stresses determination [9]

The effects that determining the internal stresses can also be related to the locking process in which forces to be transmitted will depend on the mechanical properties of the substrate and coating. Since the wetting properties of the coating are much sensitive to coating technology, materials, and parameters, the magnitude of this effect will depend on the mentioned variables. *[8]* Besides, during operations, the thermal cycle will induce residual stresses due to different thermal expansion coefficient values. Depending on the thermal expansion coefficient values different tensile or compressive stresses are expected at the different directions of the coating. [11]

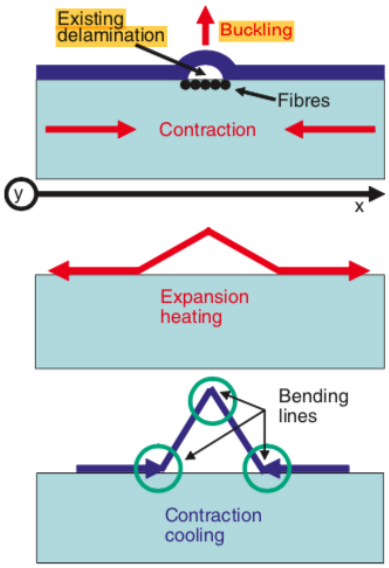

Figure 10 - Sketch of the conditions leading to buckling [11]

In this paper, the above introduction will be sufficient for the one who is interested in the refractory metals coating over graphite as PFC. Further investigations about thin film coatings are done by comparing the different experiments about the fabrication of thin films and their operational efficiencies. These experiments are selected from the literature by their topic relevance and recency. And each of these experiments is focused to improve the capabilities of PFCs. By the end of this paper, it can be expected to attain the fabrication method and material selection to obtain the most economical, reliable, and efficient refractory metal thin film coating over a carbon substrate to operate as PFC.

2. EXPERIMENTS IN THE LITERATURE

2.1. Magnetron-Sputter Deposition of W Coatings for Fusion Applications

In this experiment, the optimization of tungsten coating technology has been researched to produce coatings of tungsten with better corrosion resistance and mechanical properties. Through achieving this goal, tungsten coatings were deposited on graphite and steel substrates. The fabrication method was chosen as Magnetron sputter deposition with certain working parameters. Mechanical and tribological properties of the coatings were evaluated via Vicker microhardness, pin-on-disc sliding tests. Composition and phase evaluation was done by peak shift analysis of the X-ray diffraction patterns. Scanning electron microscopy was used to investigate the morphological properties of the coatings. As a result, tungsten thin films to have high wear and erosion resistant coatings were produced.

2.1.1. Experimental Process

In general, Magnetron sources are preferred to fabricate coatings in which a high deposition rate is necessary with having improved homogeneity, adhesion, and desired microstructure. Planar type magnetron sputter deposition was used in this project. The cryogenic pump that was controlled by the throttle valve was in use to generate a vacuum Ar atmosphere with a pressure of 10^{-6} Pa to 10^{-5} Pa with 150 $\ell \cdot s^{-1}$ pumping speed. The magnetron field is chosen to be parallel with the target to have a longer electron path around the cathode in which the ionization process is enhanced. The strength of the magnetic field is between 0.02 T – 0.04 T. Target is water-cooled which affects the energy dissipated at the cathode. And the material is 99.96% tungsten with a diameter of 7.5 cm and a thickness of 6mm. Ar ionization was done with an average of 100 eV electrons with a discharge current density of 1 $mA \cdot cm^{-2}$ to 100 $mA \cdot cm^{-2}$. Cathode – anode voltage (U) has a great impact on the discharge current. tungsten magnetron source has a low-pressure working vacuum in the range 10^{-1} Pa – 10^{-2} Pa. Other operating parameters are, substrate temperature, magnetron dissipated power, voltage, working distance, and gas pressures are also controlled. Thermocouples are attached to the sample to control the temperature with an accuracy of ±5 °C. After two minutes of deposition, the sample holder temperature was in the range of 100 °C – 140 °C with no external heating. Working parameters determined the adhesion, microstructure, and homogeneity of the films. Since the electron flux

determines the many important properties of the film the substrate is outside of the plasma zone. Control of the film growth at the surface is become a challenge due to difficulties to extract ions from the substrate. [17]

In this experiment, the working distance was chosen 3 cm – 4 cm in which the substrate was immersed in the plasma. Zero to minus 250V bias voltage was applied to obtain the value of ion current densities was up to 10 $mA \cdot cm^{-2}$. At the above 3 cm of the target Langmuir probe was set to evaluate the ion flux and electron density. The source power was -200 W and the Ar flow rate was – 1.1 $cm^{-3} \cdot min^{-1}$ and with having a substrate temperature of– 140 °C. Aspects of the Plasma are measured to be the, – $9 \cdot 10^{9}$ cm^{-3} electron concentration with -2.7 eV temperature, the sheath bias – 10 V, and the ion flux – $2.2 \cdot 10^{15}$ $cm^{-2} \cdot s^{-1}$. [17]

The stainless steel sample holder was used. graphite and stainless steel substrates for the tungsten deposition was positioned in the sample holder. X-ray diffraction, scanning electron microscope and atomic force microscope was used to determine the composition, surface morphology, and topology of the tungsten films. Wear properties of the film were evaluated by Vicker hardness and mechanical erosion tests. Adhesion of the tungsten films investigated by using Scotch tape testing. [17]

Target-substrate distance	(3 – 7) cm
Sputter gas	Ar
Magnetron discharge current	(0.1 – 100) $mA \cdot cm^{-2}$
Magnetron discharge voltage	(200 – 500) V
Ultimate pressure	$< 1 \cdot 10^{-5}$ Pa
Sputter gas pressure	(0.4 – 5) Pa
Deposition rate	(1 – 20) $nm \cdot s^{-1}$
Deposition time	(15 – 90) min
Substrate bias	0 to – 250 V
Substrate temperature	(110 – 300) °C

Figure 11 - Deposition conditions for tungsten coatings [17]

2.1.2. Results

The tungsten coatings over the steel substrate displayed good adhesion with having a thickness of fewer than 2 μm. The deposition pressure was 0.4 Pa – 2 Pa, applied bias was -50 to -150 V, substrate temperature varies – 50 ºC – 200 ºC with woking distance 5 cm – 7 cm. But, above 5 μm thicknesses of the tungsten film over steel substrates, adhesion-related failure was observed after the magnetron sputtering process with parameters of deposition rate 4 $nm \cdot s^{-1}$, 110 °C surface temperature, and 5 cm working distance. During the deposition, adhesion can be increased by having a large amount of irradiation intensity. This can be achieved via lower working distances. By having 3cm – 4cm working distances tungsten film which has a good adhesion was deposited on the stainless steel substrate with a thickness of 7 μm. ***[17]***

Adhesion between the coating and substrate may fail due to different stress states. The main stress states are; the tensile stress that affects the interface in a perpendicular direction and the shear stress is affecting the interface along the contact plane. Under stressed conditions, tungsten films may lose their rigidity rapidly than substrates which lead to failure of the substrate. If the cohesion of the substrate is lower than the adhesion at the interface the failure will be cohesive. Cohesive failure has taken place in the case of tungsten coatings over the graphite substrate. Thin films of tungsten with 1 μm – 2 μm thickness were grown over graphite with having good adhesion. However, when the thickness range becomes 5 μm – 7 μm the lack of adhesion was observed at the interface and the coatings were peeled off. This adhesion failure was different when the substrate was stainless steel. Due to weak bonding at the interface between the tungsten and graphite adhesion failure was observed in which the tungsten film was deposited via low-intensity ion radiation with a working distance of 7cm. When the ion intensity is switched to high-intensity the adhesion failure will occur at the interface because of the cohesive failure. The presence of the cohesive failure will give hint to get better adhesion between substrate and coating in which further investigations are required to solve this lack of adhesion. ***[17]***

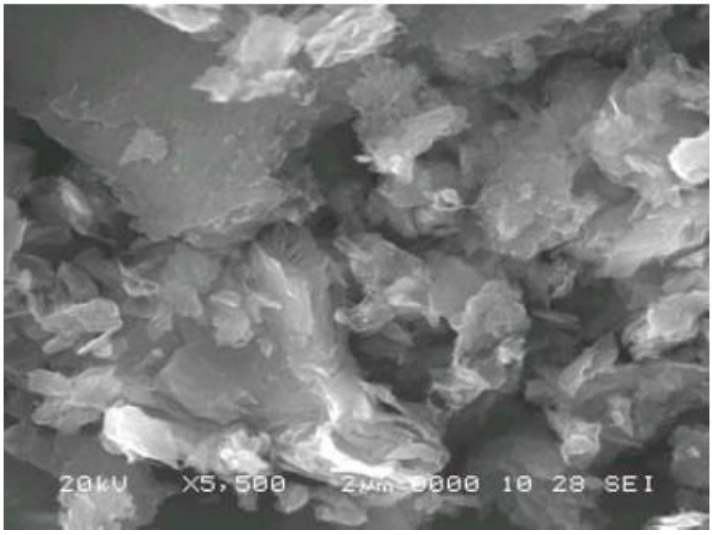

Figure 12 - Cohesive lift off of the tungsten film [17]

Scanning electron microscope analysis have shown that films were exhibited columnar microstructure. Since low adatom mobility conditions were present it was an expected result. The film microstructure can be altered by increasing the bombardment related to the negative substrate potential. For lower energy, the density was increased because of higher bombardment. As for 100 eV, 19.4 g·cm^{-3} was obtained. After 100 eV cascade collisions took place and the vacancies have formed which decrease film density. ***[17]***

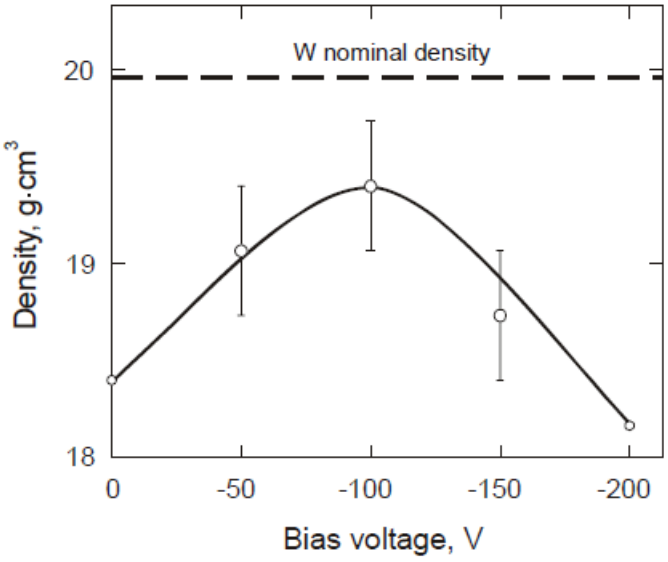

Figure 13 - Coating density – bias voltage dependence [17]

Vicker indentation method was used to evaluate the microhardness of the coatings.

V_{bias}, V	Load 50 g		Load 5g	
	h_{max}, µm	HV, GPa	h_{max}, µm	HV, GPa
0	1.36	1.4	0.42	1.4
–50	1.26	1.6	0.35	2.1
–100	1.32	2.6	0.24	5.4
–150	1.26	1.6	0.25	5.1
–200	1.29	2.2	0.30	3.2

Figure 14 - Vicker hardness measurements [17]

As a result of the Vicker hardness method, coatings which are fabricated at -100 V bias voltage have higher hardness values. The coating restructuring process could be figured out via the improvement mechanism of the coating hardness. ***[17]***

The pin-on-disk method was used to evaluate the erosion properties of the tungsten films. Parameters for the test are; applying 2.4 N to 8 N force, 10 rotations per minute, the linear speed – 8 mm·s^{-1} with 4000 rotations. The tungsten coatings over stainless steel were manufactured at 0.4 Pa,– 110 ºC, 4 cm working distance with different applied bias voltage. Thickness was 5 µm. The film fabricated by applying –50 V bias voltage has an erosion depth found to be 1 µm. When –100 V bias voltage applied erosion depth to 0.75 µm. It demonstrated that film density has also impacted over wear resistance. tungsten coatings fabricated by şon radiation of high flux and low-energy displayed better mechanical properties. ***[17]***

2.2. Manufacturing and High Heat Flux Loading of Tungsten Coatings on Fine Grain Graphite for the ASDEX-Upgrade Divertor

In this research, graphite substrates were coated with tungsten by plasma spray (PS), and physical vapor deposition. Obtained composites were tested under high thermal loads to simulate the conditions in which the PFC must operate. The failure criteria were determined by high heat flux and increasing the pulse duration. The results are evaluated to determine the critical loading conditions for each type of coating type. Structural changes of the coating were the reference point to determine the limiting loading conditions.

2.2.1. Experimental Process

Specimens were provided from different sources. One rounded edge graphite (EK98) tiles with 65x65 mm^2 area and 20 mm thicknesses were respectively coated via physical vapor deposition and plasma spray. The thermal expansion coefficient of graphite was $3.8x10^{-6}$ /K and the thermal expansion coefficient of the tungsten $4.6x10^{-6}$ /K for every temperature value. Having different thermal expansion coefficient, tensile internal stresses were expected to occur at the interface between substrate and coating. ***[12]***

Two variants of the plasma spray technique were used to fabricate coatings. These techniques were vacuum plasma spray and inert gas plasma spray. The porosity of the fabricated coatings was highly dependent on the plasma spray types and parameters. Compared to bulk tungsten, having porosities reduced the mechanical properties, thermal conductivity, and increase the hydrogen retention rate of the fabricated tungsten films. Inert gas plasma spray led to high porosity and having lamellar structures at the tungsten film compared to vacuum plasma spray. In the case of physical vapor deposition, the coatings were in a high-density state with porosity below 1% and they displayed columnar structures. Also, some specimens were subjected to a diffusion barrier which improved the adhesion at the interface. ***[12]***

Coating type	PS IPS without heat treatment	PS VPS without heat treatment	PS VPS with heat treatment (1400°C, 1 h)	PVD PVD with heat treatment (1100°C, 4 h)
Manufacturer	CEN Cadarache	KFA Jülich	P/SM AG	Plansee AG
Layer thickness (μm)	100; 200	125; 250; 375; 500	250; 500	20; 100
Porosity	15–20%	10%	8–9%	< 1%
Surf. roughness, Ra	≈ 18 μm	≤ 4 μm	≤ 4 μm	< 1 μm
Texture/structure	lamellar	isotropic	isotropic	⟨110⟩-texture
Intermediate layer	none	generally none, 1 spec. with Si	Re (PVD)	Re (PVD)
Thickness	—	50 μm	10–20 μm	10 μm

Figure 15 - List of coating from different sources [12]

Specimens were subjected to loading tests at the electron beam facility JUDITH and the hydrogen beam test at KFA Jiilich. In the electron beam facility stepwise or pulse length power density screening was implemented to specimen until it fails. The area of loading was 30 mm wide and 40 – 64 mm long. In the hydrogen beam facility, the test was performed simultaneously for 10 specimens with a heat flux of 10 MW/m' at 2s pulses for 1000 cycles.

According to the Gaussian beam profile, maximum loads were acquired at the center and the surrounding parts receive less heat flux. Ductile to the brittle transition of the plasma sprayed tungsten was expected to be in the range of 100 °C – 200 °C. After having one pulse, specimens cooled down below the ductile to the brittle transition temperature. ***[12]***

2.2.2. Results

The thermal response of the specimens was evaluated according to different pulse lengths of 1 s, 2 s, and 5 s. The temperature of the specimens was increased due to current flow through them and current flow through the specimens has formed the guidelines for determining the heat fluxes. The lowest temperature increase was observed for the 100 µm PVD, then 550 µm VPS, 100 µm IPS coating, 250 µm coating goes after. The temperature changes due to heat flux were directly related to the thermal conductivities of the coatings. 100 µm IPS coating may exhibit less temperature increase due to its lower thickness among other plasma sprayed coatings that have a negative impact over low heat conductivity. This idea was supported by a 200 µm IPS coating which exhibited high-temperature rises. However, in the case of PVD

coated films the 20 µm PVD coating displayed a higher temperature increase compared to 100 µm PVD coating and 100 µm PS coating. The metallographic inspection could explain this situation. It was observed that an excessive amount of carbide has formed which leads to a significant reduction of the thermal conductivity. Vacuum plasma sprayed coatings have a low porous structure but they have displayed a high-temperature increase which was devoted to adhesion failure at the interface of the substrate and the coating that formed a gap. [12]

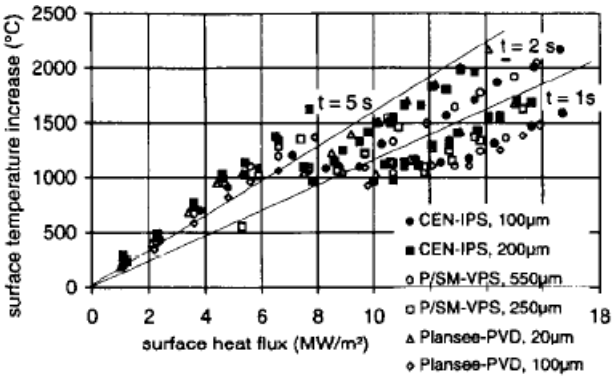

Figure 16 - Heat flux vs temperature increase of the coatings [12]

The reference equation to evaluate the performance of the coatings was found to be the maximum tolerated power density multiplied by the square root of the pulse length. This equation will help to determine the maximum achievable loads of the coatings in the environment of the divertor because the equation is proportional to the surface temperature increase. Due to different thermal expansion coefficients between the substrate and the coating temperature changes were induced thermomechanical stresses to the system. [12]

Manufacturer, coating type, thickness		$P_{A,max}$ (MW/m^2)	Δt_{max} (s)	$P_{A,max} * \sqrt{t_{max}}$ (MW/m^2 * $\sqrt{s}$)
CEN, IPS	100 μm	16.6	2	23.5
	200 μm	15.6	2	22.1
KFA, VPS	125 μm	6.3	5	14.1
	250 μm	10.6	2	15.0
	500 μm	5.5	5	12.3
VPS + Si-interlayer	375 μm	6.8	5	15.2
P/SM, VPS heat treated + Re-interlayer	250 μm	15.3	1	15.3
	550 μm	15.8	2	22.3
Plansee, PVD + Re-interlayer	20 μm	14.1	2	19.1
	100 μm	15.3	1	15.3

Figure 17- Maximum tolerated power densities of the coatings [12]

100 μm and 200 μm inert plasma spray coatings were able to reach the maximum thermal loads without displaying any degradation. However, metallographic examination demonstrated that the presence of cracks was found at the single droplets and the lamellar structure. These cracks were not able to reach the graphene substrate. ***[12]***

250 μm vacuum plasma sprayed P/SM coatings were cracked by the load of 10.9 MW/m^2, 2 s pulse length with having a 15.1 MW/m^2, 1s pulse length loading history without any observable cracking. It was expected that the crack formation started by a load of 15.1 MW/m^2. By the following pulse crack propagation started and lead to failure. Propagation of the cracks was attained by metallographic investigations. The lower damage threshold of thinner films was explained by finite element calculations in which the thinner coatings exhibited higher thermomechanical stresses compared to thicked coatings. ***[12]***

250 μm and 500 μm KFA vacuum sprayed coatings were failed because of the crack propagation and 125 μm coating was failed due to melting. Due to delamination, the melting process also took place at the flanks of the crack of 250 μm coating. Crack propagation continues until the graphite for 500 μm coatings in which failure occurs at lower loads. Unmelted impurities in the coatings were also acted as stress concentrating factors which resulted in low mechanical strength and threshold. ***[12]***

Failure of the physical vapor deposited coatings was related to crack propagation and the melting at the edge of the cracks. During the load of 15 MW/m^2, 1s pulse there were no failures. When the surface of the 20 μm coating was observed via X-ray diffraction W_2C penetration was found through the whole coating thickness due to high-temperature loadings. This indicated that the durability of these tungsten coatings was strictly dependent on carbide formations. The

Carbide layer decreased the thermal conductivity of the coating. But at very high thermal loads it was observed that mechanical properties were decreased due to carbides. The embrittlement of the coatings took place that leads to crack formation and propagation. However, 100 μm tungsten coating was not failed due to carbide formations like 20 μm thick coating. [12]

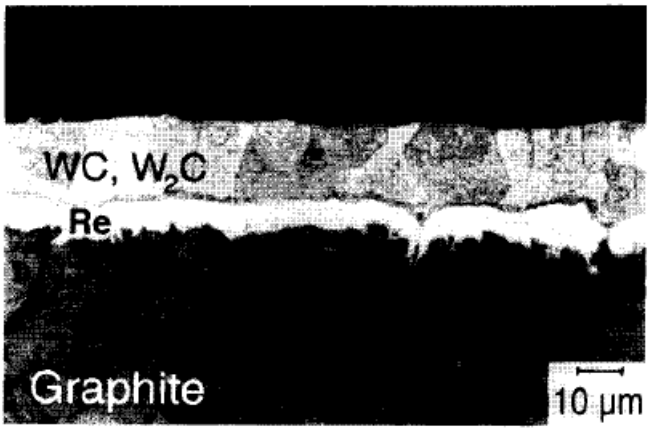

Figure 18 - Metallographic section of the 20 μm PVD coating after 14MW/m2, 2s pulse [12]

Fatigue tests of the specimens were done under different conditions. The 20 μm PVD-coating, the 550 μm VPS-coating from P/SM, the 100 μm and the 200 μm IPS-coatings from CEN coatings were subjected to 7.9 MW/m^2 average heat flux. The 250 μm VPS coatings from KFA, 250 μm coating from P/SM, and a 100 μm PVD-coating 5 MW/m^2 average heat flux. 375 μm VPS coating from KFA which contains Si interlayer was loaded with 1.8 MW/m^2 average heat flux. Delamination was not observed on any coatings. However, only the PVD coating suffered damage during the fatigue test. After 261 loading cycles, the PVD coating displayed crack formations. Subsequently, extra loading cycles formed cracks were started to propagate. By the 460 cycles, crack joints started to melt at PVD coating. [12]

Metallographic examination of the coatings was done for different types of coatings. In the case of IPS coatings, the life span of the coating was limited because of the grain growth that leads to the embrittlement of the coating at the high number of cycles. Besides, carbide formation also leads to the embrittlement of the tungsten film. Finite crack growth did not lead to any performance issues. VPS coatings did not show any significant grain growth. Only at the 550 μm coating, there was a slight growth due to high loads. Presence of the re-intermediate layer

act against the diffusion of the carbon. This feature was not only slowed the carbide formation but also controlled the formations of the carbides. As a result, carbide formation did not limit the life span of the VPS coatings. In the case of 20 μm PVD coating, the metallographic analysis demonstrated that the embrittlement of the coating occurred due to excessive carbide formation at the interface of the thin film – substrate. [12]

2.3. Carbide Formation in Tungsten Coatings on Carbon-Fiber-Reinforced Carbon Substrates

This research was devoted to evaluate the carbide formation within the tungsten and Molybdenum coatings after the heat-treatment and annealing process to estimate the kinetics of the coating degradation. The substrate was chosen to be carbon-fiber-reinforced carbon. Sample preparation was done via the focused ion beam technique. Transmission electron microscopy and diffraction patterns were used to analyze the specimens before and after the heat treatment to observe any carbide formations. [1]

2.3.1. Experimental Process

The deposition of the thin films over bi-directional CFC substrates was done via CMSII technology at the National Institute for Laser, Plasma and Radiation Physics in Bucharest. The thickness of the coating was 10 μm tungsten film layered with 2–4 μm molybdenum films. The annealing process of the sample with the dimensions of 10x3x3 mm was carried out by applying 1470K for 0.5 h, 1 h, 2 h, 5 h, and 20 h. Argon was chosen to be the inert atmospheric gas to prevent any oxidation process. Tungsten foils were used to prevent direct contact with carbon. After the annealing process, carbon diffusion kinetics from the substrate through the coating was evaluated by considering the thickness. A cross-section of the specimens was prepared by using FEI Helios NanoLab 600 dual-beam–focused ion beam/scanning electron microscopy. The correction factor was found out to be 1/cos(38°) due to the angle of beam-column which is 52°. 0.92 nA beam current for 7 minutes was used to apply platinum protection coating. The process of cross-sectioning was done in three steps; 21 nA current used to mill roughly, then consecutive cleaning carried out with 6.5 nA and 0.92 nA. In the SEM, contrasts at the image

formed due to mass differences of tungsten and formed carbide. The composition of the carbide phase was evaluated by nano diffraction in Hitachi HD-2700 Cs corrected dedicated STEM equipped with a 200 kV Schottky electron source. FIB lift-out technique was used to prepare thin lamellas to be used in STEM. A micro scratch test was carried out using the REVETEST Scratch Testing instrument which has an intender with 200 μm diamond ball to estimate the alternation of the mechanical properties of the coating because of the formation of the brittle carbide phases. Limiting load which leads to failure was found by increasing 1N to 6N with 0.05 mm/s intender speed. SEM observations were done at the FIB prepared cross-sections of the samples after the micro-scratch test. *[1]*

2.3.2. Results

Before the annealing process, as-deposited coatings were composed of 4.0±0.9 μm thick Molybdenum film and 12.7±1.2 μm thick tungsten film. The molybdenum film has been fully transformed into the Mo_2C after half an hour of annealing and the formation of a thin layer (W_2C) between Mo_2C and tungsten was observed with a thickness between 300 – 2320 nm. After 2 hours of the annealing process, the thickness of the W_2C interlayer between Mo_2C has been increased and the growth of the WC interlayer started. Further 5 hours of annealing leads to an increase in the thickness of the WC interlayer which varies from 1.2 – 2.4 μm and the total thickness of tungsten carbide reaches up to 3.2 μm. At the end of the annealing process for 20 hours WC carbide phase was in the present with a thickness of 3.3 μm and the thickness of the W_2C carbide phase was found out to be 1.1 μm and the total carbide thickness was 4.4 μm. This indicated that after 20 hours of annealing, half of the initial tungsten coating was transformed into the carbide phase.

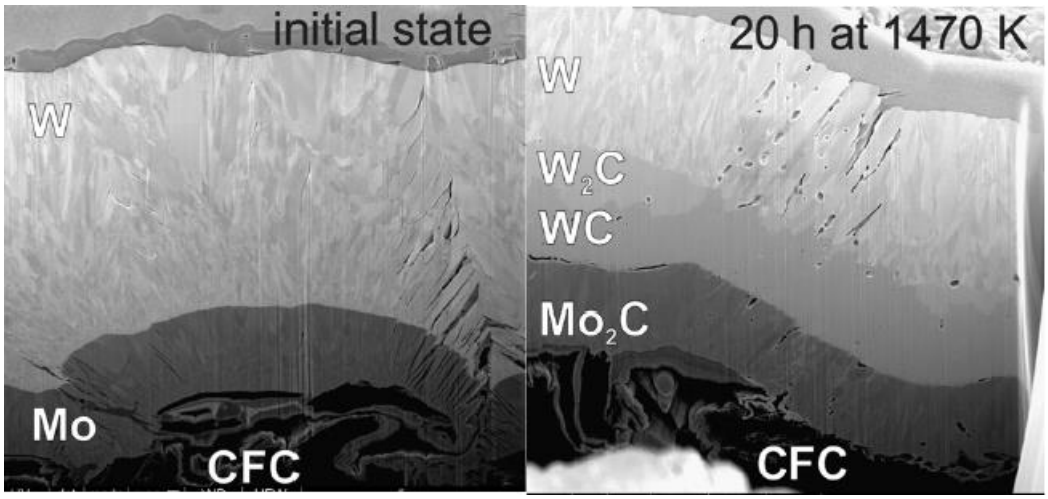

Figure 19 - Cross-section SEM images of the coatings before and after annealing [1]

W_2C carbide phase was constructed columnar grains which broaden as the annealing time with the length of 340 nm – 1020 nm and the width of 120 nm to 340 nm. Besides, it was found that the voids within the tungsten coatings are related to surface roughness and formed during the deposition process. It is an important detail that first the W_2C formed in between the tungsten and the molybdenum thin films. W_2C formed earlier than WC because it has an equilibrium carbon concentration of 3 wt.% which is lower than the equilibrium concentration of WC that is 6.12 wt.%. As the annealing time increases the carbon concentration also increases and the formation of the WC phase initiates from the W_2C phase to reduce free energy. WC phases formed as an island at the interface and they expanded as the annealing process continues until forming a continuous layer. At the early annealing times, the formation of a continuous layer was prevented by the energy of the WC – W interface. As a result, the growth of the carbide layer could be derived by the equation $d = D \cdot t^{n}$. In which d represents the carbide thickness, t represents the annealing time with an exponential factor of n and D represents the growth rate constant. The driving force of the carbide formation is dependent on n. If n is closer to 1 then the reaction rate will control the process. If n is close to 0.5 the process is controlled by volume diffusion. Total carbide layer formation occurs when the n is 0.4 which indicates that the volume diffusion controls the growth kinetics of the total carbide layer. However, in the case of WC carbide, exponential factor n is near 0.9 which means the reaction at the interface of W_2C and WC is limited by the growth rate factor. ***[1]***

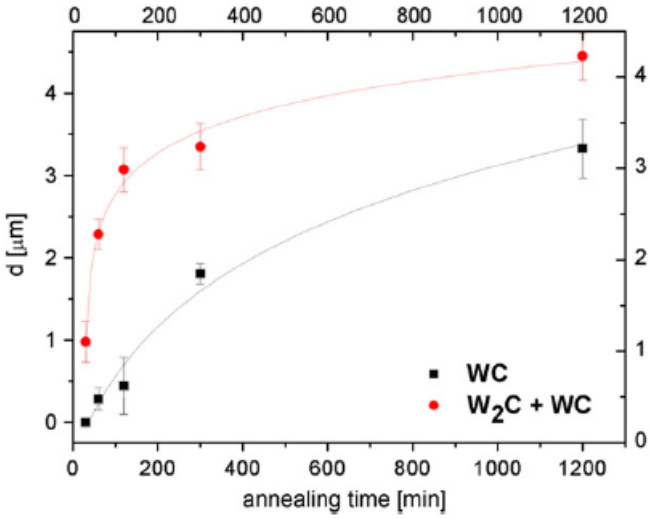

Figure 20 - Average thickness – Annealing time graph [1]

Scratch testing of the coatings was evaluated by obtaining the SEM images of the cross-sections of the coatings before and after the annealing process. Before the annealing process, some cracks were formed perpendicular to the surface but there was no failure of the coating even at the maximum force of 6 N. The coating which has annealed for 2 hours was exhibited the first failure at the scratch test under the application of 5.2 N force. Also, the first cracks were visible in the carbide layers due to 2 hours of annealing which was propagated as the annealing time. After 5 hours of annealing, the critical force which leads to failure was decreased to 4.5 N and after 20 hours of annealing, the failure force was reduced to 4.1 N. As a result, it can be said that the carbide layer has grown as the annealing time increases and this increase at the thickness of the brittle carbide layer. Since the mechanical properties of the coating were decreased due to carbide formation, the critical load which leads to the failure of the coating was also decreased. ***[1]***

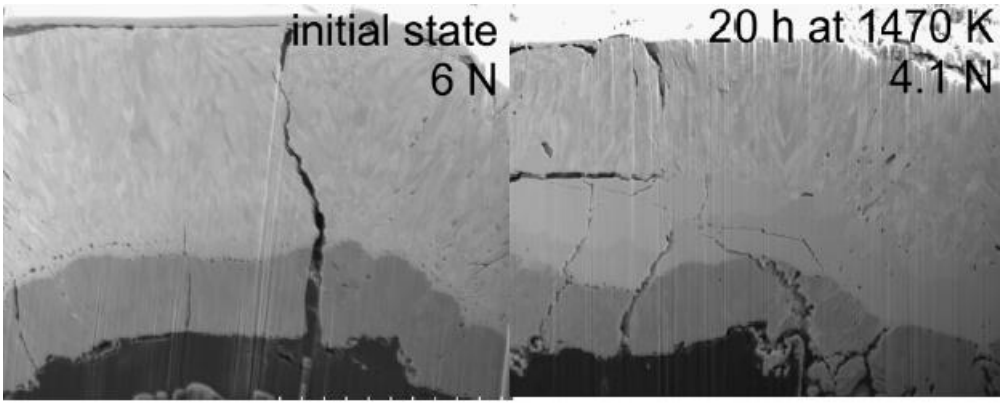

Figure 21 - Cross-section SEM images of the coatings before and after scatch test [1]

2.4. High-Heat-Flux Loading of Tungsten Coatings on Graphite Deposited by Plasma Spray and Physical Vapor Deposition

In this research, different plasma spraying techniques, and physical vapor deposition techniques were used to coat fine-graphite layers with tungsten. And these coated structures were exposed to heat fluxes to determine the maximum loading capacities of the coatings before failure. Also, the cyclic load was introduced to examine the fatigue behavior of the coatings. A comparison of the coating types and fabrication techniques were discussed to determine the best way to produce coating for high heat flux applications. ***[4],***

2.4.1. Experimental Process

Isotropic fine-grain graphite was selected as a substrate by having one round edge. The thermal expansion coefficient of the fine-graphite is 3.8×10^{-6} /K is lesser than the thermal expansion coefficient of the tungsten which is 4.6×10^{-6} /K for each temperature value. This feature will induce thermomechanical stresses at the interface of the graphite and tungsten during heat flux loads. Tungsten was coated over the round edge of the fine-graphite with different techniques. Plasma spraying was used to fabricate porous coatings and physical vapor deposition was used to fabricate dense coatings with much less porosity. ***[4]***

Porous structure due to plasma spraying will reduce the mechanical properties and the thermal conductivity of the tungsten compared to bulky tungsten and could increase the hydrogen retention. In this experiment, three different types of plasma spraying techniques were performed to fabricate coatings. The vacuum plasma spraying was used to fabricate films with low surface roughness, a thickness range of 250 μm to 550 μm by having 8 – 9% porosity. VPS was performed in a low-pressure atmosphere and subjected to a heat treatment afterward. The heat treatment process improves the microstructure of the coating by recrystallization. 10 – 20 μm intermediate layer which contains rhenium was deposited by PVD to improve the adhesion of the coating. Besides, this intermediate layer acts as a diffusion barrier and slows the pass of carbon from graphite through tungsten film. This was also slowed downed the brittle carbide formation within the coating. However, it did not prevent the diffusion of the carbon completely. As a result, the thermal treatment after the coating process was promoted the formation of the carbide layer. And 5 μm thick carbide layers were formed. Even though the thermal conductivity of the tungsten is greater than the rhenium total thermal properties of the coating did not change much due to its very small thickness. Also, coatings with a porosity of 10% and thickness of 125 μm, 250 μm, 375 μm, and 550 μm were fabricated via the VPS technique under a low-pressure atmosphere. In this case, there was no post-heat treatment which leads to a high content of unmolten particles within the lamellar structure of the coating. 50 – 100 μm thick Si-interlayer was introduced via VPS to one of the coatings to slow down the diffusion of carbon through the coating. The thermal conductivity of the silicon is similar to the thermal conductivity of the tungsten in which the thermal properties were not changed. ***[4]***

The coatings with a porosity of 15-20% with large macropores and a thickness of 100 μm and 200 μm were fabricated by inert gas plasma spray. The deposition process was carried out under a high-pressure argon atmosphere without applying post-thermal treatments and intermediate layers to the coatings. The formation of lamellar structures was observed during plasma spraying. Also, columnar grain structures can be distinguished within the droplets due to the rapid cooling of the molten particles. The surface roughness of the IPS coatings was extremely high compared to other coatings. ***[4]***

Very dense coatings with having a thickness of 20 μm and 100 μm were carried out by the physical vapor deposition technique. The surface roughness of the coating was very small. The 10 μm thick interlayer which contains rhenium was introduced to act as a diffusion barrier and a post-heat treatment was applied. The coatings were in the columnar structure. ***[4]***

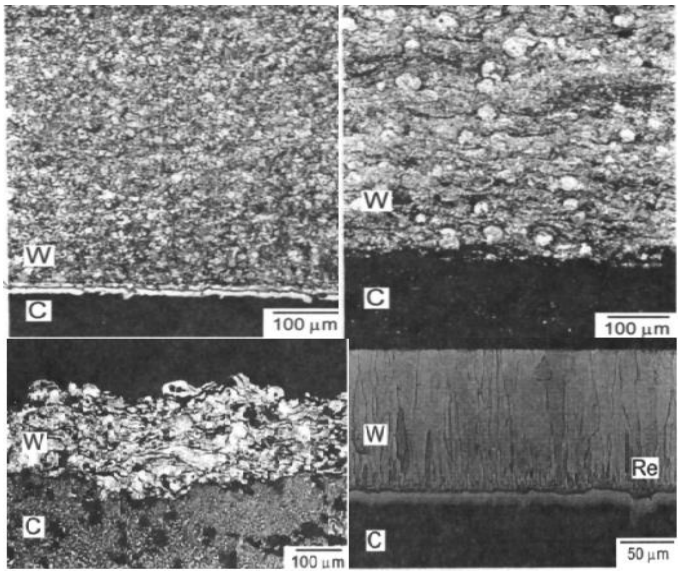

Figure 22 - Section of different tungsten coatings over graphite [4]

High heat flux experiments were carried out at the electron and ion beam facilities of Forschungszentrum Julich for determining the limits of the coatings which are expected to operate at the divertors. The screening tests were done to evaluate the threshold range which causes the failure of the coating. It was completed done by applying an increasing load up to16 MW/m^2 with 2 s pulse length maximum or until the failure occurs at the coating. The coatings which exhibited the best performances among the 10 specimens were also exposed to H-beam at the same time. And the fatigue behavior was characterized by cyclic loading tests. In which 1000 cycles were performed with a maximum load of $10MW/m^2$ and 2 s pulse length. At the cooldowns ductile to the brittle transition temperature of the tungsten coatings were passed to simulate the worst conditions. ***[4]***

2.4.2. Results

The screening test has shown that the increase at the temperature of the uncoated graphite substrate and the coated samples were found out to be similar for measured and calculated values. This similarity could be related to a good thermal agreement between the substrate and the coating which is the result of having a thermal conductivity at the same order of magnitude. Still, different temperature increases were observed for different coating types that provide

information about coating properties. In most cases, the coating which has the highest thermal conductivity exhibits the lowest temperature increase. High-density PVD coatings have the highest thermal conductivity followed by the VPS coatings with low porous structure among other types of coatings. By applying the same heat fluxes, 100 µm thick PVD coatings displayed the lowest temperature increase that is followed by 550 µm thick VPS coating, 100 µm thick IPS coating, and 250 µm thick VPS coating. The temperature increase of the 100 µm thick IPS was also at low levels. Since the 200 µm thick VPS coating exhibited much higher temperature increases compared to 100 µm VPS coatings. The low-temperature increase of the 100 µm IPS coating could be explained by its low thickness in comparison to the other plasma sprayed coatings. However, 20 µm thick PVD coating displayed a higher temperature increase compared to 100 µm PVD coating and plasma sprayed coatings especially at the short pulse lengths which was the opposite of the expectations. The metallographic examination was able to explain this with the idea of excessive carbide formation in the coating that reduced the thermal conductivity. Also, VPS coatings exhibited a relatively high-temperature increase with low porosity. [4]

Manufacturer	Coating Type	Thickness (μm)	Maximum Tolerated Power Density, P_{max} (MW/m^2)	Pulse Length, t (s)	Maximum Surface Temperature Increase, T_{max} (°C)	Macroscopic Damage
CEN	IPS	100	16.6	2	2245	---
		200	15.6	2	2245	---
PI/SM	VPS thermal treated	250	15.1	1	1629	Crack formation
	+ rhenium interlayer	550	15.8	2	2049	---
Forschungs-zentrum Jülich	VPS	125	6.3	5	2804	Melting
		250	10.6	2	1636	Crack formation, melting at flanks of cracks
		500	5.5	5	1076	Crack formation
	+ silicon interlayer	375	6.8	5	2065	Melting of interlayer, delamination, crack formation
Plansee	PVD + rhenium interlayer	20	14.1	2	2170	Crack formation
		100	15.3	1	1385	Crack formation

Figure 23 - Electron beam screening test results [4]

The metallographic investigations were completed after power loads. The damage types within the coatings related to electron beam screening were mostly the melting of the coating and the crack formations due to different thermal expansion coefficients and thermal gradients between the coating and the substrate. Also, crack propagation leads to detachment of the coating from the substrate. This resulted in melting under subsequent loads due to loss of thermal contact. The limiting loading values for each coating was also found to be different depending on the microstructure and properties. [4]

100 μm and 200 μm thick inert plasma sprayed coatings did not lose their thermal properties and they were able to stand a maximum load of 16.6 MW/m^2. Also, crack formation within the lamellar structure of the IPS coating was stuck to the single droplets that could not reach the graphene substrate. In the electron beam tests, carbide formation did not limit the thermal characteristics of the coating. [4]

550 μmVPS coating from PI/SM was able to withstand 15.8 MW/m^2, 2 s pulse length without any significant damage. This feature could relate to the fine grain orientations and the recrystallized structure. 250 μm VPS coatings were failed under the load of 10.9 MW/m^2 and 2 s pulse with a slightly delaminated spot. This load increases to 15.1 MW/m^2 with a 1 s pulse but failure at a 2 s pulse indicated that the cracks were already formed at this stage. The crack propagation through the graphite substrate was found by metallographic examinations. The thermomechanical stresses at thinner coatings are higher compared to thicker ones, this was explained by finite element calculations. [4]

Vacuum plasma sprayed coatings obtained from Forschungszentrum Julich displayed higher surface temperature increases concerning VPS coatings from PI/SM. However, their thermal conductivities were expected to be similar due to similar porosities. This difference in the temperature increase was explained by metallographic analysis in which unmolten particles reduced the thermal contact between the substrate and coating by acting as stress concentrating centers that lead to crack formations. The loading limit of the 125 μm VPS coating was found to be 6.3 MW/m^2 at 5 s pulse length and the limit of the 250 μm VPS coating was found to be 10.6 MW/m^2 at 2 s pulse length. The 500 μm VPS coating were failed at a lesser loading and formed cracks propagate through the thickness of the graphite substrate. [4]

As opposed to the theory, 20 μm thick PVD coating exhibited higher temperature increases compared to 100 μm PVD coating. This was explained by the carbide formation within the 20 μm PVD coating was faster with an exponential rate compared to 100 μm thick PVD coating.

As a result of excessive carbide formation, thermal conductivity decreased and the temperature rise was increased. Also, an X-ray examination of the coatings was done to detect the presence of carbides along with the whole thickness. Besides, the recrystallization process of the tungsten layer due to high-temperature increases observed via X-ray analysis. The limit of the100 μm PVD coating was found to be 9.7 MW/m^2 at 2 s pulse length and the threshold for 20 μm PVD coating was 14.1 MW/m^2 with 2 s pulse length. Both of the coatings were pre-loaded by 15MW/m^2 1 s pulse length without any failure. The crack formation at the PVD coatings may refer to their dense columnar grain structure. In the case of plasma-sprayed coatings, stresses due to temperature gradient and different thermal expansion coefficients were relieved by porosity. Also, the lamellar structure of the IPS coatings was able to stop the crack propagation within single droplets or change their direction. ***[4]***

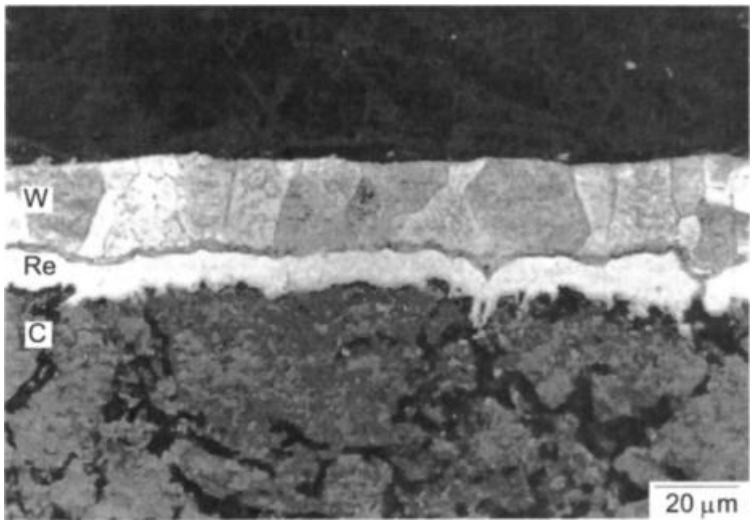

Figure 24 - 20 μm PVD coating after electron beam loading 14 MW/m2 and 2-s pulse [4]

The cyclic loading at the hydrogen beam facility introduced higher temperature increases to the coatings compared to the screening test with electron beams. At the maximum loads except the 20 μm PVD coating, no damage was observed. The damaging of the 20 μm PVD coating was due to crack formation at the end of cycle 261. Propagation of the formed cracks continues as each subsequent cycle. The melting process was observable by the 460 cycles. However, there was not any delamination occurred. ***[4]***

Manufacturer	Coating Type	Thickness (μm)	Maximum Power Density, P_{max} (MW/m^2)	Maximum Surface Temperature Increase, T_{max} (°C)	Macroscopic Damage
CEN	IPS	100	10	1590	---
		200	10	1550	---
Forschungszentrum Jülich	VPS	250	7.9	1300	---
	VPS + silicon interlayer	375	3.7	550	---
PI/SM	VPS thermal treated	250	7.9	1100	---
	+ rhenium interlayer	550	10	1675	---
Plansee	PVD + rhenium interlayer	20	10	1550	Crack formation after 261 cycles
		100	7.9	1075	---

Figure 25 - Results of cyclic loading 1000 cycles, 2 s pulse [4]

The metallographic examinations of the coatings were carried out after the cyclic loading test. In the IPS coating, the grain growth and the formation of the cracks were observed. However, these features did not lead to the failure of the coatings under cyclic loading. It was considered that the formation of the cracks related to the carbide formation within the coating. Thus the embrittlement of the tungsten layer takes place which is dangerous for the cyclic loading conditions and becomes a limiting factor. The highly porous structure of the IPS coatings acts as crack arresters that reduce the fatigue crack formation and prevent their propagation along with the thickness of the coating. As a result, crossing the ductile to brittle transition temperature did not induce significant effects on the mechanical properties of the coating. ***[4]***

The 550 µm thick VPS coating from PI/SM exhibited a slight grain growth at the highly loaded areas with a depth of 350 µm from the surface. The 250 µm thick VPS coating did not exhibit any grain growth due to less amount of heat fluxes. The diffusion of the carbon through the tungsten was greatly reduced by the rhenium-containing intermediate layer which slows the carbide formation process. Thus, carbide formation was not a limiting factor in the lifespan of their coatings. Also, the heat treatment of the IPS coatings leads to the formation of pre-existed carbides before thermal loading. This pre-existed carbide layer also acted as a diffusion barrier and slowed the further carbide formation at the coating. The coatings without an intermediate layer displayed a significant amount of carbide formation compared to coatings with a diffusion barrier. ***[4]***

The 100 μm PVD coating did not exhibit any failures under cyclic loads. However, the 20 μm thick PVD coating suffered from a crack propagation after 261 loading cycles. As a result of having a lower thickness and a high temperature at the substrate–coating interface carbide formation started at a great pace. Thus, embrittlement of the coating occurred in which the crack propagation due to cyclic loading was promoted and failure of the coating took place. [4]

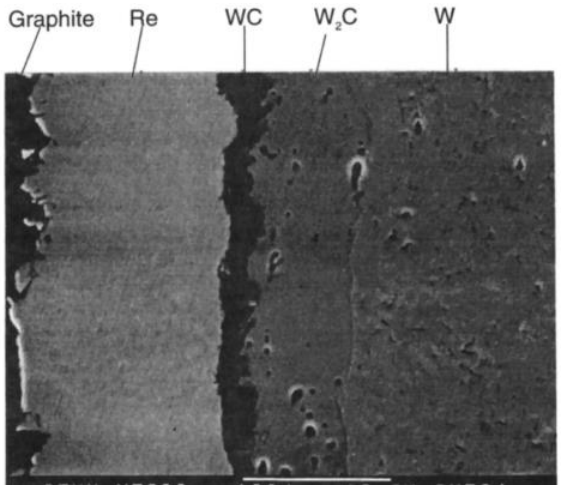

Figure 26 - Graphite/rhenium interlayer/tungsten after 1000 cycles, 550 μm VPS [4]

2.5. Thermal Performance of Multilayer PVD Tungsten Coating for the First Wall Application in Nuclear Fusion Devices

In this research multilayer tungsten and molybdenum coatings on graphite, the substrate was fabricated by radio-frequency and direct current physical vapor deposition techniques. The thermal properties of the coatings were investigated for each type of coatings by carried out experiments to evaluate thermal resistance. The microstructural changes of the multilayered coatings were also discussed to evaluate the applicability of these coatings at the first wall applications of the nuclear reactors. [10]

2.5.1. Experimental Process

The round specimens of the monoblock graphite tile which originated from KSTAR was used as a substrate having 10 mm thickness and 10 mm diameter. The physical vapor deposition technique was used to deposit tungsten and molybdenum over the graphite substrate. Planar shaped pure tungsten and molybdenum sources were used as the targets. The structure of the three different multilayer coatings was derived from the tungsten to the molybdenum ratio of the coatings which was 4:1 with a thickness of 5 μm, 1:5:1 with a thickness of 5.2 μm, and 2:1 with a thickness of 5.4 μm. The operation parameters for the PVD coating of the specimens were the same except the deposition time to preserve the crystalline structure, operating pressure was 0.007 torr, molybdenum deposited via DC at 80V, and tungsten deposited via RF via 70V. The different deposition time was used for different coatings to control film growth and reflected a small variety of thicknesses. ***[10]***

The multilayer-coated specimens with a 10 mm diameter were used in the thermal plasma chamber. The heat-flux was applied to the specimens with a ramp of 20 seconds up to 150 seconds and the loads were 1.3 MW/m^2, 2.6 $MW/m^{2,}$ and 4.1 MW/m^2 which were controlled via working distance, the torch exit, and the rate of flow of the N_2 discharge. Then samples were cooled for 30 seconds. The water cooling system with a flow-rate of 1.8 lpm was used to ensure safety at the chamber. The surface temperature of the coatings was measured by Apyrometer and K type thermocouples were used at the coolant to evaluate the heat-flux via temperature changes at the coolant. ***[10]***

The effect of the heat fluxes on the microstructure of the tungsten – molybdenum layers was evaluated by scanning electron microscope and energy dispersive spectrometer. The cross-section of the coating was the area of interest before and after the loading process. The scratch test was carried out to examine the damaging process of the coating as a result of thermal loadings. The changes in the adhesion behavior between the substrate and the coating were evaluated by the application of the scratch test. The parameters were the loading range of 0.1 N – 10 N, 100 μm diamond intender with 1 mm/min scan speed along 1mm length. The CSM scratch testing tools were used to determine the limiting loads which lead to failure of the coating. ***[10]***

Output parameter		Input parameter		
Heat flux [MW/ m^2]	Surface temp. [°C]	Target to torch exit [mm]	DC arc current [A]	N_2 flow rate [lpm]
1.3	380	140	150	150
2.6	685	70	170	170
4.1	1285	50	170	160

Figure 27 - Experimental parameters of the heat flux test [10]

2.5.2. Results

The tungsten layers were suffered from 4.1 MW/m^2 thermal loading and displayed crack formations. Because of the limited control of the plasma torch apparatus, copper contaminants were found at the surface of some coatings. However, this contamination did not lead to any significant morphological changes between the coatings under thermal loads. ***[10]***

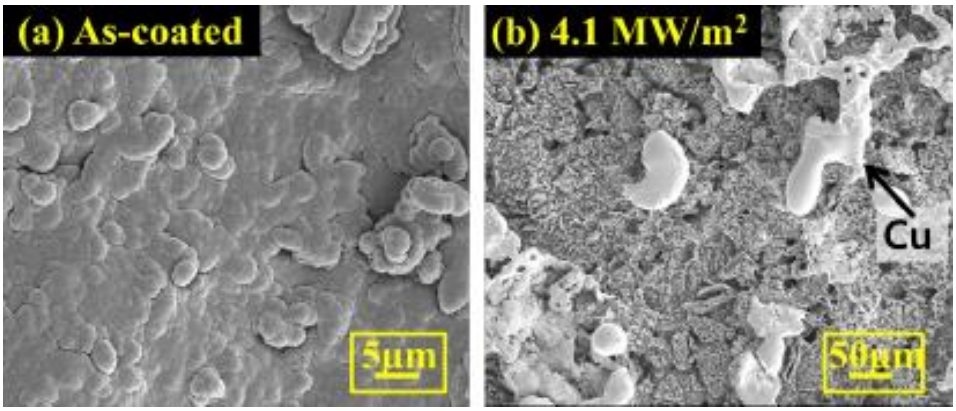

Figure 28 - Surface morphology of the single layer tungsten – molybdenum coating [10]

The coatings have displayed similar microstructures near the center of the cross-sections due to the uniform distribution of the thermal loads around the center. The coatings did not fail as a result of 1.3 MW/m^2 thermal loading and the microstructures were not changed visibly. But the changes at the microstructures were visibly initiated after 2.6 MW/m^2 loading depending on the layering types. Single layered tungsten – molybdenum was displayed crack formations at the substrate – coating interface after 2.6 MW/m^2 loading. By the 4.1MW/m^2 heat loading, formed

cracks were complete their propagation through the cross-section. Duble layered tungsten – molybdenum did not exhibit significant microscopic changes. At the 2.6 MW/m^2 some minor crack formations took place. However, by the end of 4.1 MW/m^2 loading, these cracks did not propagate through the cross-section. Triple-layered tungsten – molybdenum coatings suffered from a significant amount of delamination and failure has occurred after 4.1 MW/m^2 loading. ***[10]***

In general, the tungsten coatings that were fabricated by physical vapor deposition contain residual stresses which leads to intergranular fracture. If the PVD coating was produced to have a columnar structure with a small grain size the failure mechanism may start at the coating – substrate interface or inside the coating due to high loadings. This experiment conducted that single layer tungsten – molybdenum coating suffered a cohesive failure and triple layer tungsten – molybdenum layer exhibit a failure mode of adhesion. The modes of the different failure types were not certainly clear. In this case, the adhesion mechanism was dominated via mechanical interlocking, it presumed that presence of the molybdenum interlayer was act as interlocking sites and improved the adhesion. Also, molybdenum interlayers reduce the change of the thermal expansion coefficient in which the residual thermal stresses were decreased. ***[10]***

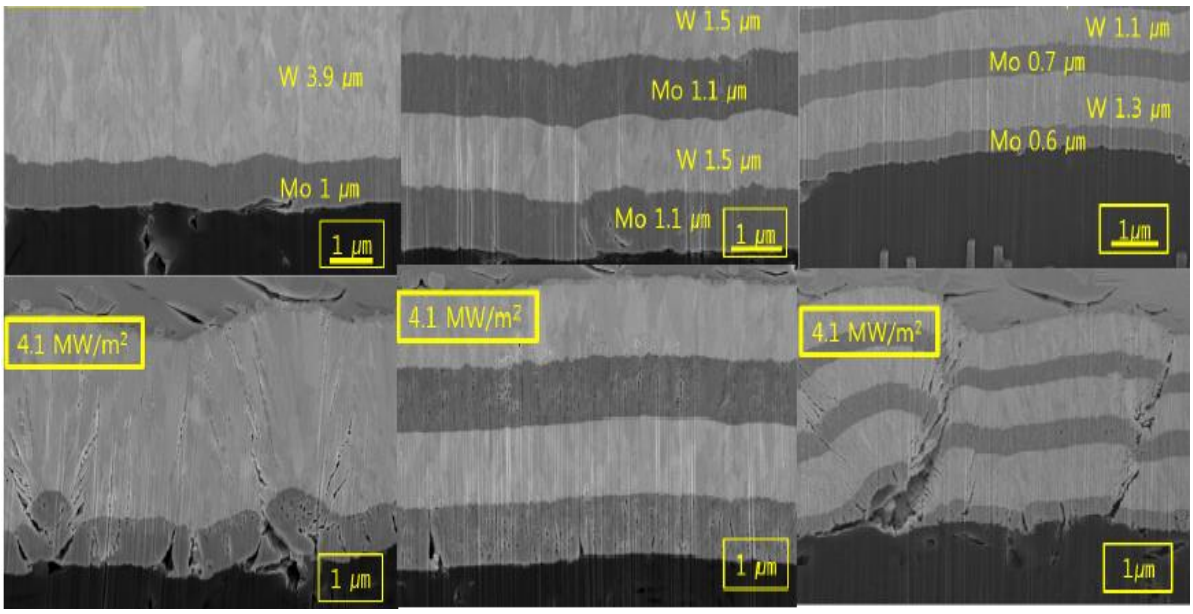

Figure 29 - Cross-sections of the coatings as pre-coated and after 4.1MW/m2 load [10]

The adhesion of the coatings to the substrate was examined by the scratch test. The loads that lead to crack formation and the complete propagation of the cracks within the specimens were evaluated. Complete crack propagation was considered a failure due to the lack of adhesion as a result of the applied critical load. The adhesion of the coating was found to be greater if the necessary force related to complete crack propagation is larger. The critical load for the as coated double layer tungsten – molybdenum was found to be the largest, triple layer tungsten – molybdenum layer has the second-largest critical loading, and the single layer tungsten – molybdenum coating exhibited the lowest critical loading. As the thermal loading increased the critical loading values to have failure was also decreased except for the double layer tungsten – molybdenum coating. The drop of the critical load for the triple layer tungsten – molybdenum coating at the load of 2.6 MW/m^2 was very steep. Also, for the 1.3MW/m^2 thermal load, the decrease of the critical load was not significant. It was concluded that microstructural analysis and the scratch testing results were in a parallel direction to evaluate the changes within the coatings after thermal loadings. ***[10]***

By comparing the double and the triple layer tungsten – molybdenum coatings (each layer contributed) the effect of residual stresses due to insufficient thermal compatibility was observed. Also, the number of the multilayers was not important but the thickness of the layers was found to be important for the adhesion of the coatings. It can be concluded that the structure of the interlayer linked the relation between energy absorption and failure conditions. ***[10]***

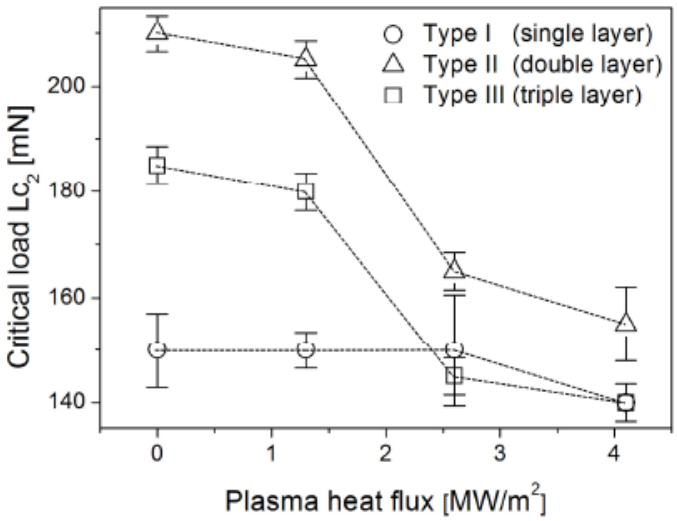

Figure 30 - Scratch test critical loads for each coating [10]

2.6. Investigation of Tungsten Coatings on Graphite and CFC

In this research, the deposition of the tungsten on the carbon substrates was done by vacuum plasma spray and physical vapor deposition total of fourteen coatings. The coatings were fabricated with having different thicknesses of 4, 10, and 200µm. The produced coatings were subjected to thermal loading via screening, cyclic and edge-localized tests. Afterward, metallographic examinations, X-ray diffraction measurements, and the evaluation of the adhesion of the coatings were tone to determining the causes of the failure at different types of carbon substrates. ***[11]***

2.6.1. Experimental Process

As for the graphite substrate, in this experiment, the reference material was chosen as SGL R6719 by having a thermal expansion coefficient of 5.8×10^{-6} K^{-1} and the thermal conductivity of $100W(mK)^{-1,}$ and the back-up material was Schunk FP479 used with a thermal expansion coefficient of 6×10^{-6} K^{-1} and thermal conductivity of $100W(mK)^{-1}$. The bulky tungsten has a thermal expansion coefficient of $4.9x10^{-6}$ K^{-1} in the temperature range of 20 – 1000 °C.

Reference and back-up graphites were coated with tungsten as 200μm vacuum plasma sprayed layer combined with PVD deposited tungsten – rhenium layer to form an interlayered structure that exhibited a variety of porous structures. In the interlayered architecture, the highly porous structure was able to relieve stresses thus, it resisted crack formations. Besides, the denser structure exhibited higher thermal conductivity. Also, reference-grade graphene was coated by VPS with a 120 μm thick tungsten layer with a single rhenium-containing interlayer that was deposited by VPS at 30 μm thickness. ***[11]***

The carbon fiber composite substrate was chosen as 2d-CFC Dunlop DMS780 which has a thermal expansion coefficient of 10^{-5} K^{-1} at the x-direction and 0 K^{-1} at the y-direction. Since the difference between the thermal expansion coefficients of tungsten and CFC were at the order of magnitudes the heat flux test was carried out with new parameters. The fibers of the CFC were oriented at the y-direction and z-direction which was perpendicular to the surface (1^{st} layout). Also, another CFC sample was fabricated with parallel planes to the surface (2^{nd} layout). In this way, an isotropic later thermal expansion coefficient was obtained. However, by changing geometry thermal conductivity was reduced to 70 W $(mK)^{-1}$ from 230 W $(mK)^{-1}$ at room temperature. So it was tested by application of lower heat fluxes. Also, thick and thin tungsten coatings were coated over CFC with different techniques gathered to obtain many test information as possible. These fabrication methods were PVD, VPS, and CVD that leads to different microstructures. ***[11]***

Supplier	Technique	Interlayer	Thickness (μm)
Coatings on CFC			
Plansee AG, A	PVD	–	2–6
DIARC Techn., FIN	PVD	–	3–5
DIARC Techn., FIN	PVD	Re	5–7
Archer Technicoat Ltd, GB (ATL)	CVD	–	7–8
WTCM, B	CVD	–	4
Plansee AG, A	PVD	–	11–13
DIARC Techn., FIN	PVD	–	8–14
MEdC, RO	PVD	Mo (II)	10–13
Archer Technicoat Ltd, GB (ATL)	CVD	–	12–14
WTCM, B	CVD	–	4–10
Centro Sviluppo Materiali, I	VPS	TiC	230–250
Plansee, A	VPS	W/Re (SW)	220–240
St.Gobain, F (StG)	VPS	Re	190–260
Archer Technicoat Ltd, GB (ATL)	CVD	Re	240–250
Coatings on graphite			
Plansee AG, A	VPS	W/Re (SW)	220–240
Sulzer-Metco AG, CH (SM)	VPS	Re	150

Figure 31 - Testing specimens [11]

2.6.2. Results

The 200 µm VPS tungsten coatings over CFC and graphite (R6710) were subjected to the screening test to evaluate the thermal response of the specimens. Also, it was found that by applying short-pulses the temperature increase at the surface of the graphite samples was higher than the CFC samples due to the lower thermal conductivity of the substrate. During the cooling process because of the large contractions of the CFC coatings, crack formations were observed. This phenomenon leads to a failure by delamination of the CFC coatings with the deposition of 200 µm VPS, 200 µm and 10 µm CVD, and 4 µm and 10 µm PVD. It was observed that the thin coatings of the CFC substrate were suffered from its non-homogeneous surface. The VPS tungsten coatings with a back-up graphite substrate exhibited melting at maximum heat flux load as a result of the low thermal conductivity of the substrate. ***[11]***

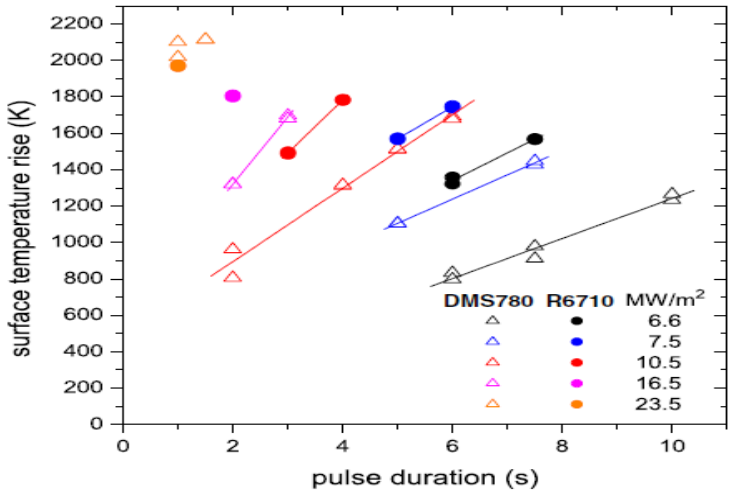

Figure 32 - Thermal response of the 200 µm VPS coatings [11]

The specimens which were able to pass the screening test exposed to cyclic loading with 10 MW/m^2 with a pulse length of 5 s for CFC and 3.5 s for graphite substrate. 200 loading cycles were carried out, in this way, the fatigue behavior of the coatings was examined. The 200 µm CFC coatings have exhibited delamination at the millimeter scale and some of them have failed. VPS coatings were suffered from unmolten particles which act as stress concentration zones, delaminations at the sharp edges which was also increased the stresses at this zone. However, the graphene substrate tungsten coatings did not fail due to cyclic loading. The crack

propagation at some millimeters was observed because of the stress relaxation but it did not lead to any significant damage to the coating with round edges. The thick coatings have shown better thermal performance compared to thinner ones due to their high heat capacity and strength. ***[11]***

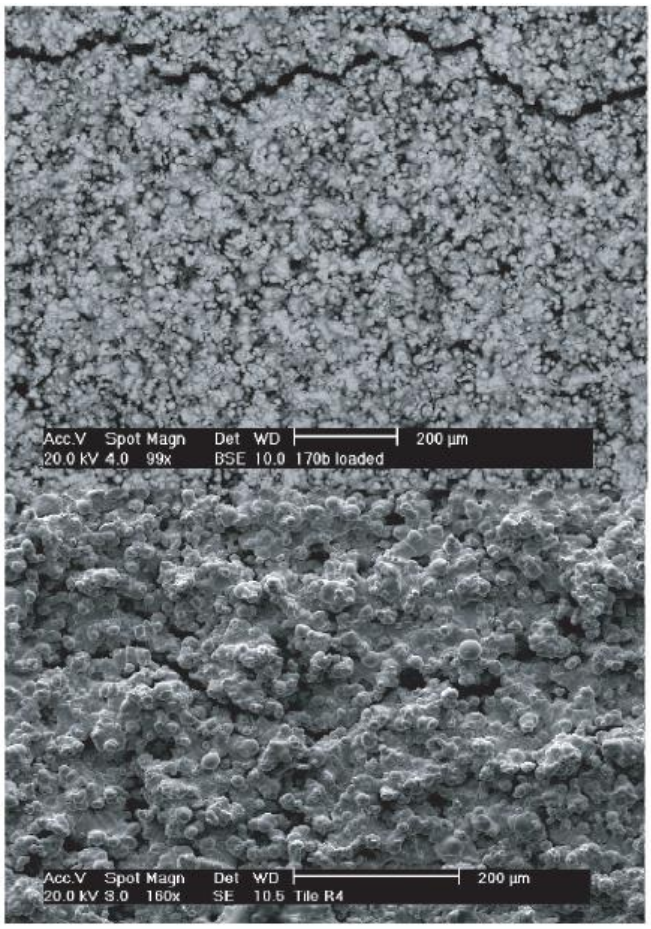

Figure 33 - SEM image of VPS coatings over CFC(top) and graphite (bottom) [11]

In the first layout of the CFC substrate, the fibers were oriented at the y-direction of the surface. During the increase of the temperature, the expansion of the coating was larger than the substrate at the y-direction and less at the x-direction. As a result, when the temperature rises the coating has been exposed to tensile stress at the x-direction and compressive stress at the y-direction. At the room temperatures, PVD coatings displayed compressive residual stresses in all directions Then, any temperature increases were reduced the compressive stresses at the x-direction but increased the compressive stresses at the y-direction which may lead to failure. In reality, due to temperature increase stress relaxations occurred at the coatings because of the

plastic deformations or re-crystallization precesses that are thermally activated. Consequently, the pulse length and numbers are important at the value of the heat flux that was applied to the coating. After obtaining a low-stress structure, the cooling process has taken place that affected the system oppositely. The compressive stress appeared in the x-direction and tensile stresses appeared in the y-direction which exceeds the tensile strength of the coating in the y-direction. The formation of the cracks that were observed with parallel to x-direction. Distance between cracks was also decreased by the coating thickness. For 200 μm coatings the crack distance was 4 μm and as the coatings get thinner this spacing was shifted to 100 μm. *[11]*

Because of the low-cycle fatigue phenomenon, thin CFC coatings have failed by the 200^{th} cycle with respect to fibers at the y-direction. The presence of compressive stress due to substrate contraction leads to the buckling-out of coating at the areas in which the adhesion is insufficient. This compressive stress at the coating was inversely proportional to the thickness of the coating. Also, thinner coatings were less rigid than the thicker ones and bend easily which leads to buckling. Hence, the buckling was taken place in one lateral direction even at the low heat fluxes even 5 MW/m^2 heat flux was not low enough to prevent buckling. Besides, pre-existed buckles were also experienced heating cycles and they also felt bending forces that lead to plastic deformation and crack propagation within the coating. The prevention of buckling was done by increasing the stiffness of the coating that could be achieved by increasing the coating thickness. *[11]*

The evaluation of the adhesion of coatings was done by gluing a stainless steel cylinder with a 1 cm diameter to the coating. Afterward, the tensile testing machine was used to pull the cylinder until the coating peels off. The maximum adhesion values for the thin coatings were not reliable due to the porous structure of the substrate in which the glue could penetrate and form interlocking sites. Besides, failure was observed due to the lack of adhesion. As for the thick coatings, the adhesion test was reliable because the glue could not penetrate through the surface. The CVD and VPS coated specimens exhibited very high adhesion with peeling of stress up to 19MPa due to sufficient mechanical interlocking between the substrate and the coating. In the case of the graphite substrate, maximum stresses were found to be 29.2 for R6710 and 24.3 for FP479. *[11]*

The $\sin^2\varphi$ method was used to evaluate the in-plane stresses at room temperature. It was quantified by an X-ray diffraction peak. The PVD coated samples were found to be in a compressive stress state. Also, magnetron sputtered PVD coatings exhibited high compressive stresses due to the high-velocity impact of the clusters of atoms to the surface. The CVD

coatings exhibited direction-dependent stress states. The thick coatings were displayed low isotropic tensile stresses in which the stress levels at the sub-surfaces extracted due to penetration depth restrictions of the instrument. [11]

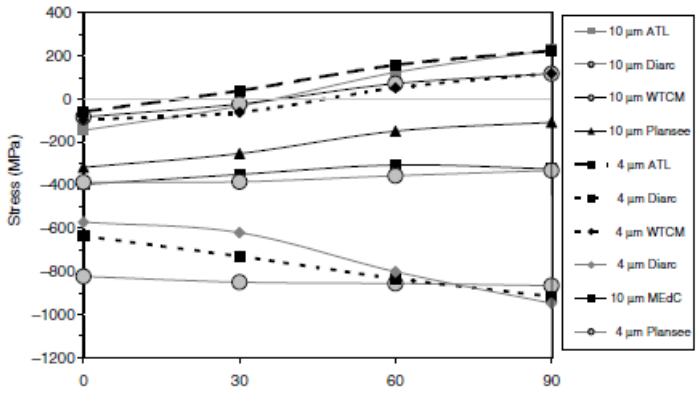

Figure 34 - Stress state of the thin coatings at room temperature [11]

2.7. The Properties of The Tungsten Coating on Fine Grain Graphite Using Pulsed Laser Deposition

In this experiment, the graphite substrate was successfully coated with tungsten by the pulsed laser deposition technique. The microstructure of the tungsten coating was evaluated to define its properties. Cracks or gaps within the coating were investigated with respect to contamination levels. And the stress-state of the film was determined according to the parameters of the pulsed laser deposition. The lattice strains and grain size changes were determined via X-ray diffractions and Rutherford backscattering spectroscopy to evaluate the residual stresses at the coating. [3]

2.7.1. Experimental Process

The tungsten and the graphite samples were placed within the vacuum chamber in the pulsed laser deposition machine. At the null state, the back-pressure of the chamber was 1.3×10^{-4} Pa and it was obtained via turbopump and diaphragm pump. The incident angle of the laser beam was 45° by having a triangular shape. However, the value of the back-pressure of the chamber

was increased to 2 Pa during deposition due to the purge of Argon gas with the mean free path of several centimeters which leaves some spaces for the laser beam for penetrating the tungsten. ***[3]***

The deposition time was set to 4 hours. And as a laser, krypton-fluoride was used to obtain a beam with a wavelength of 248 nm and an energy of 600 mJ. The duration of the laser pulse was 20 nm by frequency of 20 Hz. The laser was focused over a 2.5 mm^2 tungsten target that leads to the fluence of 20 J/cm^2 and homogeneous evaporation of the tungsten was obtained by covering the whole surface area. The working distance was chosen as 5 cm from the tungsten surface. The graphite was preheated to 800 °C for 1 hour to remove any trapped gas within the substrate, then it was decreased to 500 °C in a controlled environment to have a good deposition. The type substrate was chosen as R6710 with dimensions of 2 cm diameter and 5mm thickness that exhibits low crackings as exposed to thermal heating due to its thermal expansion behavior. The surface roughness was measured by the profilometer before and after the deposition as a function of distance. The surface was found to be smoother after the deposition. ***[3]***

2.7.2. Results

The thickness of the tungsten layer that was deposited over the graphene substrate by the pulsed laser deposition technique was evaluated by the Rutherford backscattering spectrometry and SIMNRA software. In the literature, by using the RDS method, a non-destructive evaluation of the thickness, the composition, and the elemental depth of the different tungsten coatings was done. As operation parameters, 1.7 MW 5SDH Pelletron Tandem was used to analyze the coatings that are normal to 2 MeV α-particles. The backscattered particles with a scattering angle of 165° were detected via the Passivated Implanted Planar Silicon detector (14 keV energy resolution and 25 mm^2 areas) supplied by Canberra. The thin layers of gold over silicon and chromium over silicon-oxide was used to calibrate ion beam energy with 3.034 MeV O(α,α) resonance. Due to the interaction between the beam and the materials in which the loss of energy took place, the highest energetic particles were ejected from the surface and followed by near-surface zones. The carbide formations or the substrate roughness was determined by the low energy tail of the tungsten signal. The thickness of the tungsten layer (90% tungsten) was evaluated concerning the energy of the laser beam which was around 150 nm for below 500 mJ

laser energies and increased up to 300 nm for higher laser beam energies with a coating rate of nearly 4.75 nm/min. [3]

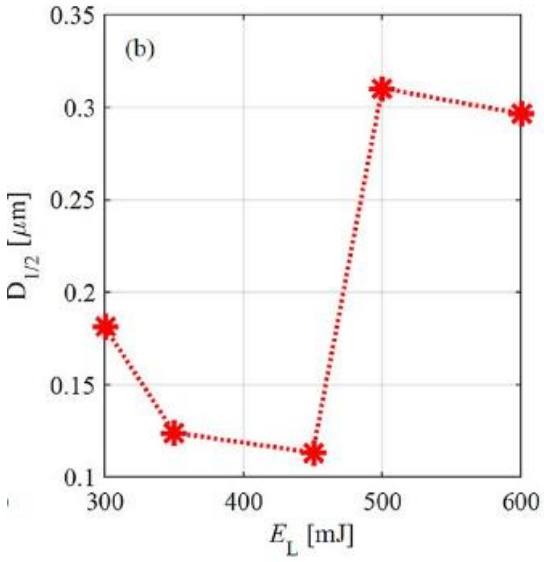

Figure 35 - Coating thickness vs Laser beam energy graph [3]

The morphology of the tungsten layers which were deposited by parameters 500 mJ, 2 Pa argon pressure, 20 Hz pulse frequency, and 4 hour deposition time with PLD was evaluated by scanning electron microscope at different magnifications (MIRA3 TESCAN). The tungsten was shown in light gray color and the graphite was shown in dark gray color with a uniform coating. At the higher magnifications, it was observed that there were no cracks or holes at the interface which indicated a good adhesion between the tungsten layer and the graphite substrate. [3]

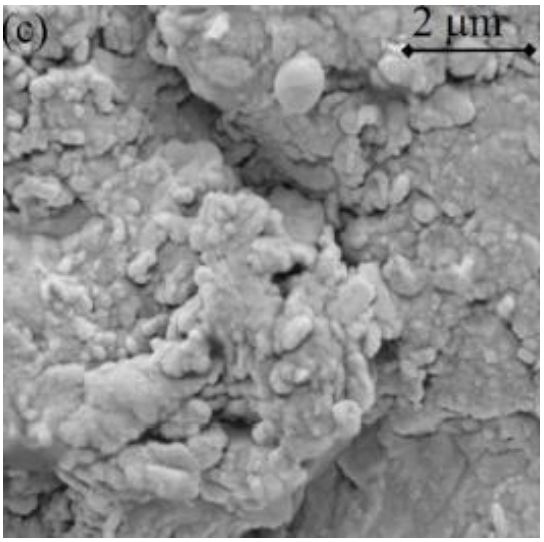

Figure 36 - SEM image - top view of the tungsten coating [3]

The sample was cut through the cross-section direction and placed within SEM to observe the tungsten – substrate interface by scattering and back-scattering electrons. In the SEM, the electrons were accelerated by 10 kV with a working distance of 12 mm. Since the BSE was sensitive to the atomic number, the conclusions with SE were not clear and reliable. Then, the examination of the deposited layer was done and coating thickness was found to be 300 nm. ***[3]***

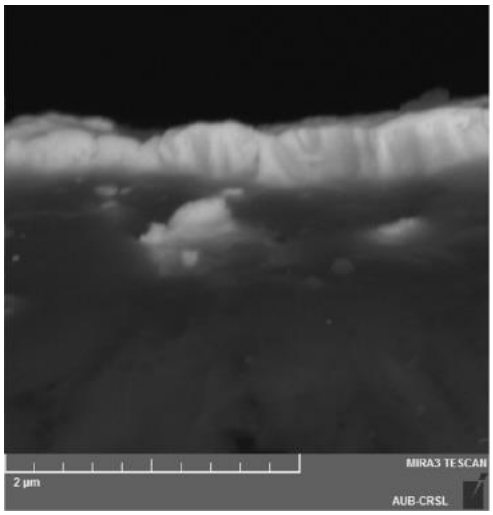

Figure 37 - SEM image of the coating, tungsten (light) – graphite (dark) [3]

The constituent analysis of the coatings was carried out via X-ray spectrometry. The imaging of the coating was displayed by different coloring. The graphite substrate was illustrated red, tungsten coating was illustrated blue and the oxygen was illustrated green. The spectrum lines were also created by X-ray intensity as a function of wavelength to detect oxygen contamination of the coating. By examining the line intensities, the concentration of different elements was evaluated as a function of depth due to electron beam energy. With the increase of the beam energy of the PLD from 300 mJ to 600 mJ it was observed that the tungsten film region at the coating was increased to 95% from 87%. The decay length of the electron beam was increased due to higher coating rates by filling the gaps of the substate with tungsten. The contamination percentage of the coating was also examined to finding a relationship with an electron beam voltage. However, it concluded that the oxygen content was 1% for all of the electron beam voltages it only increased if the vacuum back-pressure is higher. [3]

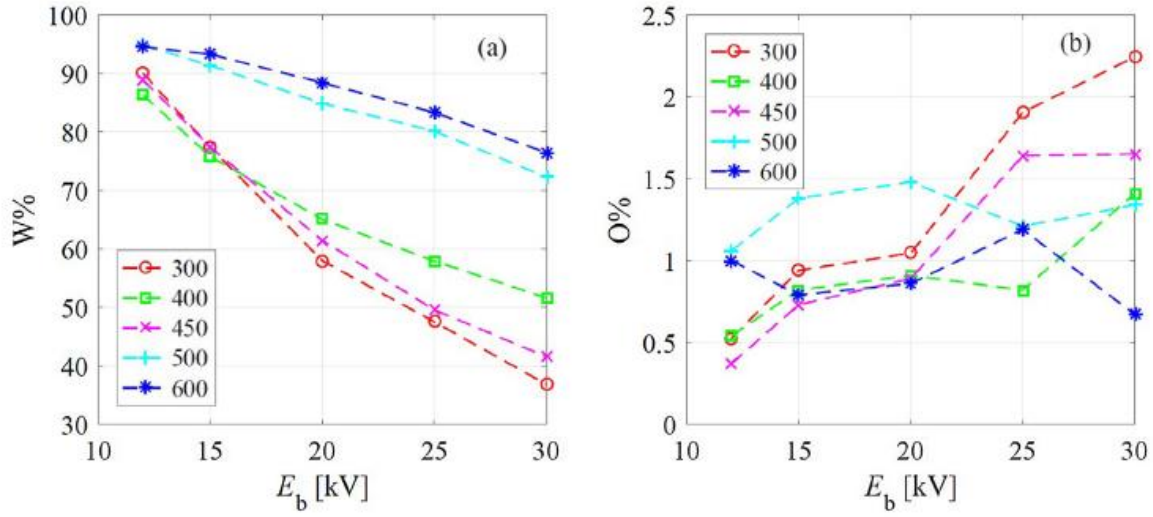

Figure 38 - Material content – electron energy graph [3]

The X-ray diffraction was also used to examine the structure of the tungsten coating. Information about the spacing of layers, the orientation of grains, crystal structure, and the straining of the planes was extracted via the XRD method. The XRD peaks of the graphite have occurred at 42.4°, 44.4°, 54.4°, and 77.5° before the coating process. After PLD coating of graphite with tungsten for 4 hours and 20 Hz frequency, new peaks appeared at 40.3°, 58.3°, and 73.2° by having (110), (200), and (211) crystalline orientation. It was concluded that the

tungsten coating was in crystalline form and exhibited a BCC structure with 0.317 nm unit cell length (the sum of each peak was even) on top of the hexagonally structured 0.246 nm unit cell length graphite substrate. The (110) and (211) oriented planes were chosen to determine the structural properties – laser energy relation. The angles at (110) direction shifted to lower values that demonstrated the strain present in the tungsten lattice at the tensile form ($\Delta D/D>0$). As the energy of the beam doubled the amplitude of the peaks was also increased by five folds. This broadening at the peak was occurred due to the finite size of the mono-crystals and the lattice dimension changes of the BCC structured tungsten lattice over the hexagonal lattice graphite. When the energy was increased to 600 mJ from 300 mJ the crystallite size increased 20 nm. Also, the effect of the back-pressure affected crystallite size which may lead to amorphous latticed films. The lattice strains were increased to $3.6x10^{-3}$ from $1.9x10^{-3}$ as the laser beam energy goes to 400 mJ from 300mJ for further energies straining decreased to $2.5x10^{-3}$.s[3]

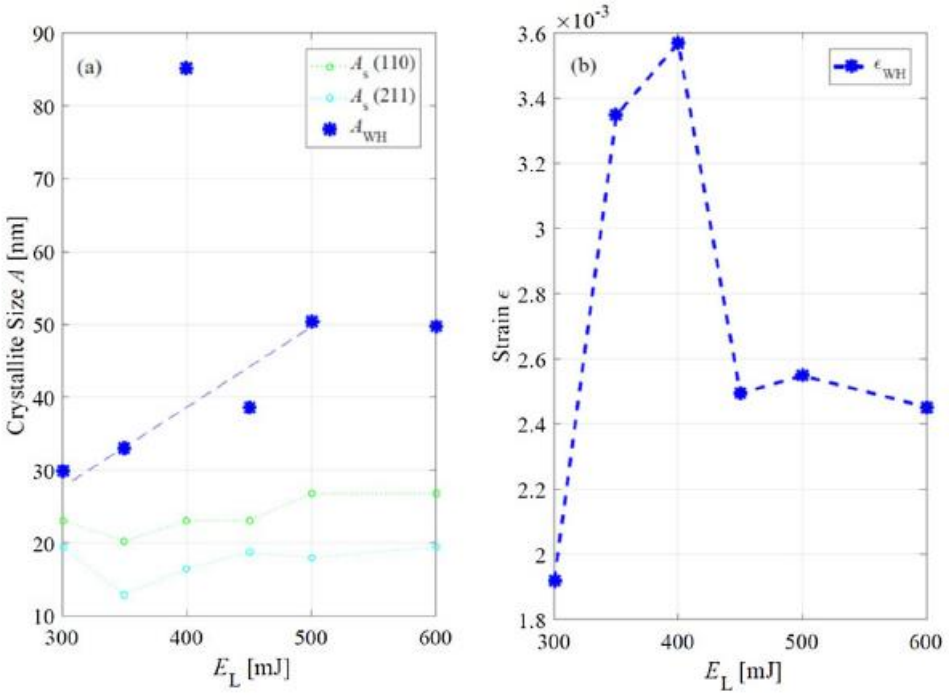

Figure 39 -Crystalline size / Strain vs laser energy graphs [3]

2.8. Manufacturing of Tungsten and Tungsten Composites for Fusion Application via Different Routes

This research evaluated different techniques to fabricate tungsten materials. The powder preparation, bulk densification, additive manufacturing, and coating technologies were investigated. However, attention was only paid to the powder preparation and coating technologies. And the properties of the tungsten materials were presented for further research.

2.8.1. Experimental Process

Powder Preparation & Results

In the plasma spray deposition process to obtain an advanced tungsten coating, the powder preparation step of the tungsten is very important which determines the characteristics of the coatings. Because many of the structural properties; purity, homogeneity, forming fine grains are depends on powder preparation of the tungsten. The powder preparation of the tungsten could be done via a top-down approach or a bottom-up approach. At the top-down approach, the particle size and shape were altered and refined grains were formed due to cold welding, plastic deformation, and cracking processes. In the bottom-up approach, the wet-chemical method is dominantly used to induce second-phase strengthening to tungsten by reduction of the precursor and adding allowing or second-phase particles. Re, Ta, V was used as doping alloying elements to prepare tungsten alloys by the mechanical milling process in which the transfer of kinetic energy from milling balls to the powder occurred. As a result, mixed, heated, and deformed mechanisms contribute to the homogeneity of the powder that contains a different type of elements. In the literature, it was demonstrated that W – Cr – Y powder was alloyed after 60 h of the milling process. Also, it was shown that the wet – chemical method was used to produce nanoscale powders. Oxide contamination in the powder preparation process is generally difficult to control due to oxygen affinities of the alloying elements and contaminations due to millings balls are also inevitable that reduces the mechanical properties of the material. The amount of retained deuterium may increase and dust production may also increase due to carbon presence Besides, nanoscale tungsten matrix composites with having second–phase of TaC, TiC, etc. were produced by mechanical milling that exhibits great mechanical properties. It was found that W – TiC composite produced by wet – chemical

process exhibited better mechanical properties compared to mechanical milling because of having fewer contaminants. The solid-liquid doping and liquid-liquid doping concepts are also important in the wet – chemical process. [22]

It was concluded that, by mechanical milling high surface roughness, fine grain size, and high residual stresses were observed after the densification process with high sintering driving force but low flowability. In the case of the wet – chemical process the morphology, size distribution of the particles were dependent to process parameters and the mass production of the powders was easier with the wet – chemical method. [22]

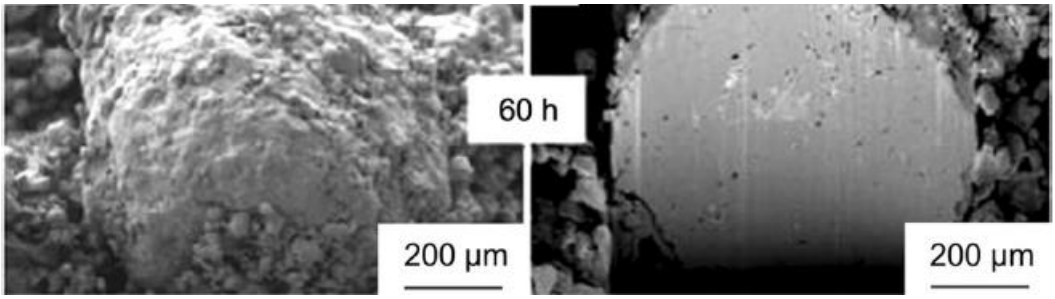

Figure 40 - The cross-section of a large particle after 60h of milling [22]

Coating Techniques & Results

It was announced that the thickness of the tungsten-containing coating PFC at the walls of divertors must not exceed 3 mm. Thus the tungsten coatings were fabricated by vacuum plasma spray, chemical vapor deposition, and atmospheric plasma spray. Besides, tungsten coatings could be applied directly via heat sinks. It demonstrated that high-density tungsten coatings with excellent thermal resistance were fabricated by the chemical vapor deposition technique. Because the grains of the coating could elongate by having larger grains normal to the substrate. The coating may have a hardness of 300 – 400 HV. However, CVD exhibits very low deposition rates of about 0.6 mm/h. Thus it is not feasible for mass production. The coatings produced by the atmospheric plasma spray method exhibited high oxygen contamination which was reduced by adding LaH_2.[22]

2.9. Recent Research and Development of Thick CVD Tungsten Coatings for Fusion Application

In this project, tungsten coatings were fabricated by atmospheric pressure chemical vapor deposition. Then microstructures of the tungsten coatings were observed with respect to annealing processes. The thermal stability and shock resistance were evaluated for fusion device applications. The effect of surface polishing was examined and different crack thresholds were obtained for each coating type. Besides, APCVD tungsten coatings were exposed to deuterium and fission neutron to simulate irradiation performances of the coatings. Also, large-scale fabrication of tungsten-based plasma facing components was found to be worth mentioning.

2.9.1. Experimental Process

The CVD coatings of the tungsten were fabricated by hydrogen reduction of volatile metal halides (WF_6) and the pyrolysis of the carbonyl. It was more convenient to use the hydrogen reduction of the volatile metals inside the reaction chamber to produce larger-scale coatings. The purity of the reactant gas, in this case, WF_6, was very important for the quality of the coatings. WF_6 gas was purified by multi-step processes up to 99% from the very high impurity percentages. By this purification step and the management of the exhaust gas, the cost of the tungsten coating fabrication via CVD becomes too high. ***[21]***

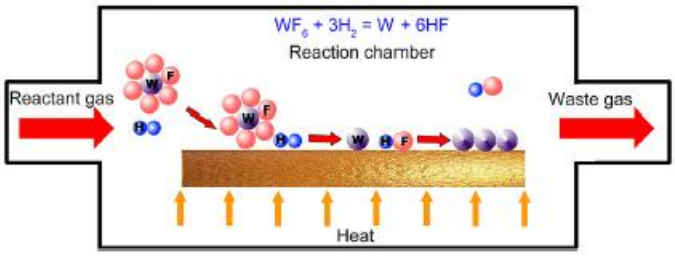

Figure 41 - Schema of tungsten coating via CVD [21]

The drawbacks were overcome via the APCVD process in which high deposition rates (0.4 – 1.0 mm/h) were observed with lower costs. The highly corrosive HF was the exhaust gas of the reaction. The danger of environmental pollution due to exhaust gas was prevented by using soda lye. APCVD technique was used to fabricate tungsten coating with copper-based, carbon-based, and molybdenum based materials. The copper-based substrates were more preferable due to its relatively easy removal by melting. The shape of the tungsten coatings fabricated by APCVD were complex-shaped cylindrical shells, conical tubes, and flat-tiles. Inert gas fusion was used to determine the oxygen and nitrogen content of the coatings. The sample was burned by oxygen to determine carbon content and glow discharge mass spectroscopy was used to detect other element contents.

Element	C	Element	C	Element	C	Element	C
C	<5	Al	0.03	Cr	0.08	Ni	0.02
O	<10	S	0.02	Fe	0.01	Zn	0.02
N	<5	Ca	0.03	Ti	0.002	Co	0.008
Ta	<1	Hg	<0.1	Re	<0.05	F	<0.01
Th	<0.0001	U	<0.0001	Others	<0.38	W	Matrix

C is the concentration of an element with a unit in wt. 10^{-4}%

Figure 42 - Chemical compositions of CVD tungsten products [21]

2.9.2. Results

The density of the CVD coated tungsten was 19.23 g/cm^3, calculated by the water immersion technique. The thermal diffusivity of the tungsten in the range of 200 °C – 1000 °C was calculated by 12.7 mm and 3.5 mm diameter and thickness by TM – 5000 and a comparative method was induced to predict specific heat. By obtaining density, thermal diffusivity, and specific heat the thermal conductivity of the tungsten coating was found out to be comparable with pure tungsten and larger than forged tungsten. The thermal expansion coefficient of the tungsten coating was determined for 500 °C – 1300 °C by a vertical dilatometer. As a result, the thermal expansion coefficient of the CVD tungsten was higher than forged tungsten at the

200 °C – 670 °C range. On contrary above 670 °C, the thermal expansion coefficient of the forged tungsten was higher than CVD tungsten. The change of the thermal expansion coefficient was also smoother for CVD tungsten which means higher thermal stability. [21]

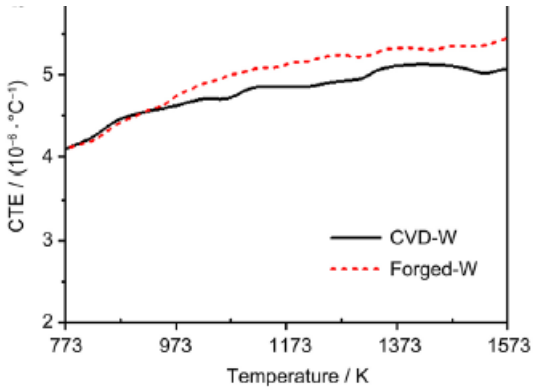

Figure 43 - Thermal expansion coefficient vs temperature graph [21]

The microstructure of the CVD tungsten contained the clues of high thermal conductivity. SEM was used to examine the surface of the CVD tungsten material. The roughness of the CVD tungsten was found to be very high by composed of pyramidal shapes and the roughness was increased as the thickness of the CVD tungsten coating. The mechanical polishing process was necessary for a millimeter range thick coatings to reduce the roughness. The polished sides of the CVD tungsten were investigated by an optical microscope and it was found that highly oriented columnar grains were formed along the direction of the thickness that may reduce the heat flow. Also as the thickness increased, the grain width increased too by having larger than 100 μm grains. The weak points of the columnar grains along the thickness may also present a good path for crack formation and propagation. [21]

The tensile test and Vickers hardness tests were done to investigate the mechanical properties of the CVD tungsten coatings. The Vickers hardness was found to be 416 HV which is close to wrought tungsten by applying 1.96 N force for 30 s with a diamond pyramid. The uniaxial strain tests were done for 200 °C and 400 °C after cutting the samples normal to the thickness. At 200 °C CVD tungsten exhibited a low tensile strength (columnar grains) and very small plastic deformation that exhibited brittle behavior. Testing at 400 °C showed that the brittle behavior of the CVD tungsten was decreased and tensile strength reached 200 Mpa. [21]

It was expected that the microstructures of the CVD tungsten altered due to high temperatures in the recovery, recrystallization, and grain growth modes. It was shown that the Vickers hardness of the coatings was affected by the annealing temperatures. If the annealing temperature was below 1500 °C the Vickers hardness was also decreased slightly. The annealing process at 1500 °C showed that the grain size of the CVD tungsten was less than 10 µm which meant no recrystallization. The significant decrease at the Vickers hardness occurred above the annealing temperature of 1500 °C due to the grain growth mechanism. Besides, as the annealing time increased for the recrystallization process the thermal stability was found to be better than rolled pure tungsten. The storage energy of the high annealing temperature samples was also high with perpendicular grain growth to the thickness. Also, TEM images have shown that the dislocation tangles and flat grain boundaries were present at the annealing temperatures below 1900 °C, and the loops were still in presence up to 2300 °C that approved great thermal stability. ***[21]***

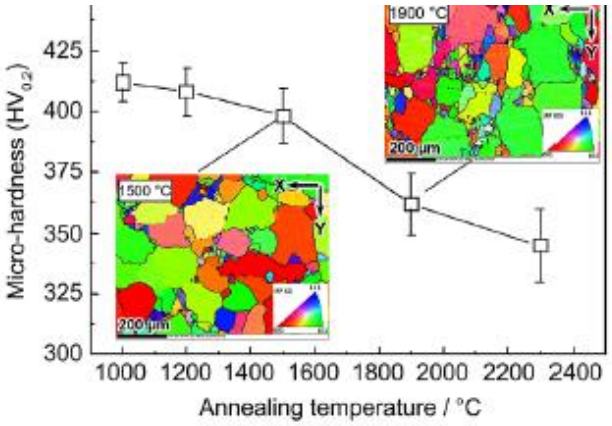

Figure 44 - Vickers hardness vs annealing temperature graph

The effect of the thermal flux was investigated for CVD tungsten by the electron beam device with 60 kW. It was observed that the surface morphology and having a columnar grain had a great impact on the thermal resistance of the CVD tungsten. 0.16 GW/m^2 to 1 GW/m^2 power densities were used for 5 ms pulse durations to simulate disruption loadings for polished CVD tungsten and rolled tungsten. The limiting power density for cracking was 0.30 GW/m^2 for CVD tungsten and this value was reduced to below 0.22 GW/m^2 for rolled tungsten. Besides, it was found that the polished CVD tungsten presented higher resistance for cracking compared

to high roughness surface CVD tungsten. The CVD tungsten was exposed to the thermal loadings with 0.16 GW/m^2 to 1 GW/m^2 by 1ms pulse lengths for 100 cycles with a surface temperature of room temperature to 600 °C. The cracking threshold for the as-deposited CVD tungsten was lower than 0.16 GW/m^2 at room temperature with a roughness of 16.7 μm that induced stress intensification at the pyramidal structures. Moreover, this cracking threshold was increased up to 0.44 GW/m^2 for polished CVD tungsten due to low contamination (reduce embrittlement), strong texture through (200), great thermal conductivity due to columnar grains, and high purity. The high-temperature annealing also had an impact on the thermal shock resistance. 2300 °C annealed CVD tungsten the cracking threshold was decreased to 0.16 GW/m^2. [21]

The plasma irradiation resistance of the CVD tungsten and rolled tungsten was investigated by plasma surface interaction studies. The materials were subjected to deuterium plasma with a peak flux of $1.5x10^{24}$ and fluence of $6x10^{24}$ ions/m^2s^2 up to 290°C. It was observed that the CVD tungsten exhibited great plasma irradiation resistance compared to rolled tungsten in which only a few deuterium blisters were found on the whole surface compared to many blisters on the rolled tungsten surface. Also from the X-ray diffraction results, it obtained that as-deposited CVD tungsten had a monophasic body-centered cubic phase that wakens as the thickness grows. In the case of polished CVD tungsten, strong texture at the (100) direction was observed which improved the blistering resistance of the coating. Besides, hardening embrittlement and the decrease of the thermal conductivity were observed at the CVD tungsten due to neutron irradiation that leads to voids and vacancies but it is still comparable to wrought tungsten. [21]

In the literature, there were many types of research to apply CVD tungsten coatings into plasma facing components. The CVD tungsten coating over graphite mockups was successfully fabricated with having PVD deposited silicon layer to prevent carbon diffusion into the tungsten coatings. The CVD tungsten coating was deposited up to 1.38 mm/h. And this coating was successfully withstood 4.62 MW/m^2 power density with 5 s pulse length for 200 cycles during the fatigue tests by having a surface temperature of 1800 °C. Although some melting processes occurred at the pyramid-like grains, no delamination or cracking was observed. [21]

2.10. Properties of Tungsten Coatings Deposited on Graphite by Vacuum Plasma Spraying Method

In this experiment, the deposition of tungsten coatings over the graphite substrate was performed by vacuum plasma spraying technique consists of sand-blasting, pre-heating, and post-treatments. One of the coatings was also contained an interlayer to prevent carbon diffusion. Besides, the properties of the fabricated tungsten coatings were investigated via the Vickers hardness test, XRD, EDS, and FE-SEM. The heat loading test was applied to evaluate the thermal response of the tungsten coatings.

2.10.1. Experimental Process

The setup of the vacuum plasma spraying was consisting of a direct current torch (a few thousand K temperatures) in which the plasma formed between the central cathode and annular anode. The coating material was purged into plasma and melted in-flight then hit the surface of the graphite. Trajectory and the parameters of the plasma spraying exhibits a great impact on the coating properties. The VPS chamber had a plasma gun with 55 kW power output, 4 kg/h feed rate powder feeder, a vacuum chamber, a pressure between 10 mbar – 900 mbar, and a plasma gun manipulator. *[21]*

The graphite substrate was chosen to be isotropic (CX-2320) with dimensions of 50 mm x 50 mm x 30 mm. The target was the powder of tungsten with a 9.40 μm size due to its high melting point. The carbon diffusion layer was chosen to be a titanium interlayer deposited via vacuum plasma spraying before the tungsten coating to slow down the carbide formation. The plasma was formed by helium and hydrogen gasses with 37.1 kW power. Argon gas was also used in pre and post-treatment processes. The surface roughness and temperature had an impact on the wetting process. High temperature and roughness provide additional wettability. Before the coating process, the graphite surface was cleaned via sandblasting than annelated above 1100 °C to increase wettability. After annealing, the coating of tungsten over the graphite substrate was carried out. The post-heat treatment was applied to form a stable microstructure by controlled cooling. The surface roughness and Vickers hardness tests were performed to evaluate the mechanical properties of the tungsten coatings. The field emission scanning

electron microscopy was used to determine the surface morphology and coating thickness. X-ray diffraction and energy dispersive spectrum was carried out to investigate the compositional changes of the materials. The heat loading test was carried out by a VPS applying 10 MW/m^2 load with pulse lengths of 10 s, 30 s, and 60 s. The ablation resistance was determined after the analysis of the microstructure. ***[21]***

2.10.2. Results

The thickness of the tungsten coating with a titanium interlayer was found 378 μm in which the titanium layer had an average thickness of 28.6 μm (formed evenly on the substrate) and the coating without an interlayer was found to be 409 μm thick. There were not any delamination or crack formations observed. By the outcome of the energy dispersion spectroscopy at the coating boundary, diffusion of the tungsten and carbon atoms were observed that expected to form the tungsten carbide at high temperatures. In the case of a titanium interlayer, very low carbon diffusion from the substrate to coating was observed in which the titanium layer acted as a diffusion barrier. The crystal structure of the coating was examined by X-ray diffraction. It was found that no change in the crystal structure was observed for tungsten before and after the coating process due to controlled VPS carried out under inert gas and no environment interactions. The surface roughness of the coating was calculated as 4.35±0.07 μm for 10 random data. As a result of the Vickers hardness test, the hardness of the titanium layer containing tungsten coating was found to be 77.2% of the bar-type bulk tungsten and the hardness of the tungsten coating without an interlayer was found to be 82.4% of the bar-type bulk tungsten. ***[21]***

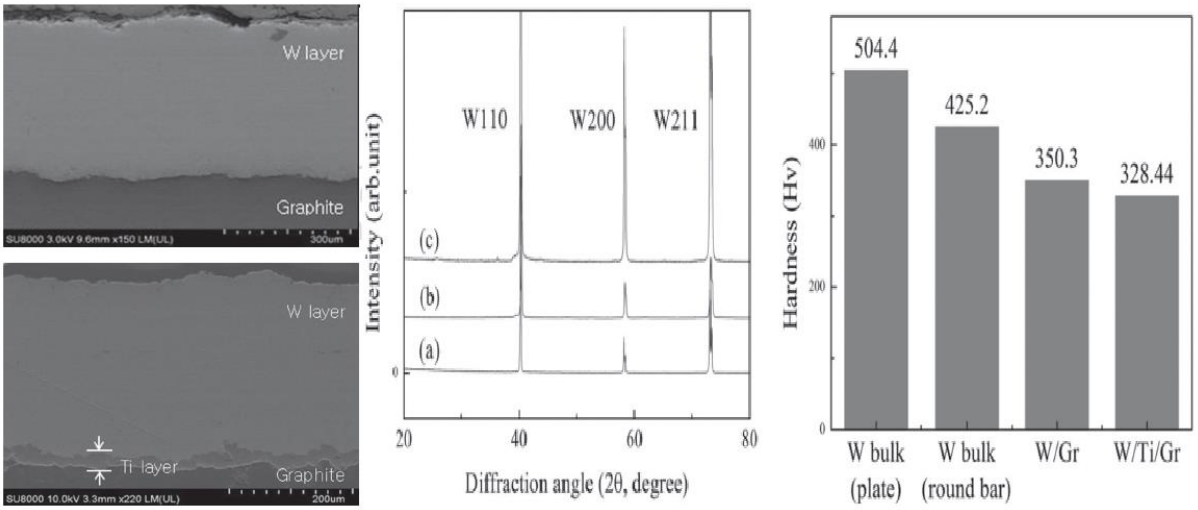

Figure 45 - SEM images, XRD and Vickers tests of the coatings [21]

The layers of the coating were examined by FE-SEM after the heat loading test. It was observed that tungsten particles were joined after melting and exhibited both lamellar and columnar structures. The presence of the micro and nano-sized pores were examined which formed due to gas trapping and the size of these pores was increased as the test time increase. Also, the carbide formation rate was increased for each type of coating. But no crack or delamination took place after the heat loading test for coatings with or without containing a titanium interlayer. ***[21]***

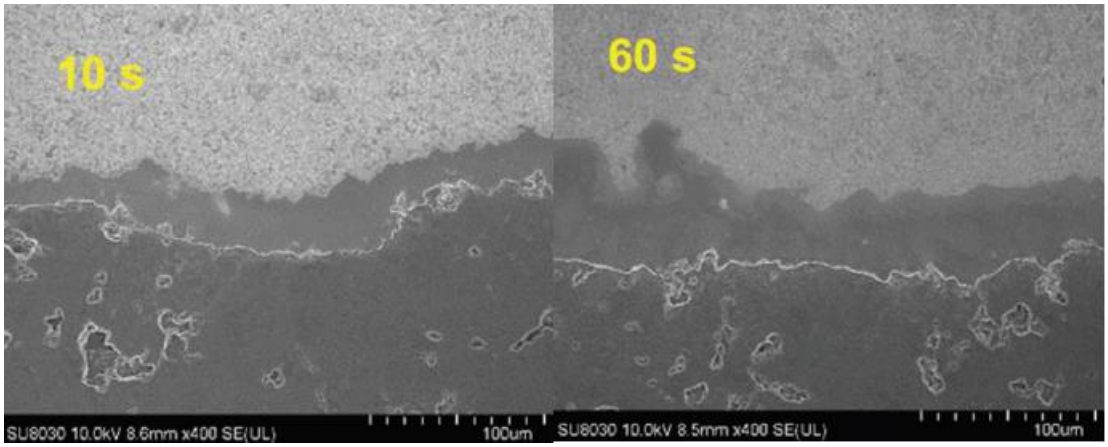

Figure 46 - SEM images of titanium interlayered coating at heat loading tests [21]

2.11. Properties of Tungsten Coatings Deposited onto Fine Grain Graphite by Different Methods

In this research, tungsten was coated onto the graphite by electron beam evaporation, magnetron sputtering, and arc deposition methods by the thickness of the micrometer range. Their properties were compared for fusion applications, impurities within the coatings were evaluated. Thermal heat loading tests were performed to examine the thermal behaviors of the coatings.

2.11.1. Experimental Process

The tungsten coating process by electron beam evaporation was carried out under 2-3x10^{-7} mbar pressure and 150 °C substrate temperature with a deposition rate of 0.2 nm / s. The thicknesses of the coatings were 200 nm to 500 nm (determined gravimetrically) with a surface roughness of 1.5 μm. The tungsten coatings by arc deposition had 1 μm to 10 μm thicknesses with the same surface roughness as the electron beam evaporation technique (milling pre-treatment) over R6710 and FU4204 graphite substrates. The tungsten coating by magnetron sputtering was taken place at an argon atmosphere with a pressure of 3x10^{-3} mbar. The etching thickness of the target was 0.8 μm and the temperature of the substrate was controlled by radiative heating. The maximum coating thickness was found to be 3 μm if the substrate surface was pre-treated via etching process and the coating done immediately after etching, if not the maximum achievable coating thickness was 1 μm with good adhesion. Otherwise, for thicker coatings, the delamination occurred in form of small flakes with 1 mm size. Since the delamination process was found to be independent of the deposition temperature it concluded that the coatings were under compressive stresses for all temperature ranges. The stress state of the coatings was related to the deposition atmosphere which was 3x10^{-3} mbar. [14]

2.11.2. Results

The scanning electron microscope was used to examine the tungsten coatings which were fabricated via different techniques. The conformal coverage of each coating and fabrication method was excellent. The X-ray photoelectron spectroscopy was used to determine the content of the light impurities. In the case of magnetron sputtered tungsten coatings, 5keV argon ions with 0.6 – 0.8 μA used to determine the light impurity content until it reaches the top content value. It was found that the carbon content was near 5 at.% and the oxygen content was below 1 at.% for both magnetron sputtered and arc deposited tungsten coatings. In the case of electron beam evaporated coatings the carbon content was average 7.5 at.% and the oxygen content was average 12 at.%. This difference may be attributed to the growth rate of the magnetron sputtered and the electron beam evaporated coatings. Also, the surface topology of the three different coating types was different. The evaporated and sputtered coatings exhibited a columnar structure with intrinsic surface roughness and the arc deposited coatings were denser and had smoother surfaces. [14]

The scotch tape test was used to evaluate the adhesion of the tungsten coatings that were fabricated via different methods. When the electron beam evaporated coatings were pre-heated for the 0.2 μm – 0.5 μm thickness no delamination was observed. If no polishing was applied the delamination occurred. In the case of magnetron sputtered coatings, no delamination was observed at 0.5 μm thickness. The arc-deposited coatings did not exhibit delamination up to 10 μm independent from the substrate material. [14]

The heat flux experiments were done by an electron beam of 120 keV (40x31 kHz). The thickness of the coatings must exceed 1μm to absorb this energy. The temperature of the surfaces was measured with a two-color pyrometer with 550 °C to 1760 °C. The power of the fluxes was between 2 MW/m^2 and 22 MW/m^2 with 0.5 s ramp up and down and 2.5 s nominal value. Delamination was observed for the sputtered coatings with 3 μm thickness and 150 °C coating temperature due to the presence of the tensile stress. No delamination occurred for high temperature deposited coatings. The cracking took place throughout the 20 – mm substrate at 17 MW/m^2 due to the flaw of the substrate. Otherwise, no cracking was observed. The finite element analysis was used to evaluate the melting temperature for 1 μm thickness with 18.7 MW/m^2 load and was found to be 2800 °C. [14]

2.12. Tungsten–microdiamond composites for plasma facing components

In this paper, microdiamond tungsten was used in the composite material in comparison to nanodiamond. The thermal conductivity of the nanodiamond was better than nanodiamonds due to photon transport capabilities. But, as the positive attributes increased also the carbide formation from the microdiamond increased.

2.12.1. Experimental Process

Mechanical alloying was used to produce different tungsten microdiamonds by W-40% microD powders. The matrix was pure tungsten and the size of the microdiamond powders range from 10 μm to 100 μm to be used as reinforcement. The milling process was carried out 2 hours and 4 hours for 10 μm, 50 μm, and 100 μm batches with a 10 mm tungsten carbide planetary ball mill. The rotation speed was 200 rpm. SEM, X-ray diffraction, optical microscopy, dispersive X-ray spectroscopy, and differential thermal analysis were used to characterize the powder batches. The samples were in an inert argon atmosphere for heating and cooling with a rate of 293 K/min. The laser flash instrument was used to determine the thermal diffusivity. Spark plasma spraying was used to consolidate the milled powders at the temperatures of 1073 K, 1123 K, 1273 K, and 1423 K. Characterization of the consolidated samples was also carried out like the powder sample and a Vickers test addition. [19]

2.12.2. Results

The XRD has shown that the tungsten carbide formation was prevented via the milling process by containing a very small amount of tungsten carbide due to ball mill contamination. 4 h milling time was produced more homogeneous diamond particles with a uniform size distribution compared to 2 h milling process. This was also applicable for consolidated samples by spark plasma spraying. The thermal analysis of all batches has similar conclusions. 100 μm sample exhibited endothermic peaks at 1423 K due to the graphitization of diamond and in the

range of 1243 K to 1253 K due to tungsten carbide formations (both WC and W_2C). The endothermic peak formation was shifted to lower temperatures for high milling durations. The densification of the material was sufficient after spark plasma spraying consolidation. In the case of microD at 50 μm, 4 h milled, and 1273 K spark plasma spraying, the geometric density was 77% and the hardness was 13.67± 2.79 GPa. The hardness for the low-density materials which consolidated below 1273 K was very low to measure. The hardness was increased for high-temperature consolidation temperatures due to tungsten carbide formations. The thermal conductivity of the materials was proportional to their density. It was expected that the high consolidation temperatures should give better thermal conductivity. However, above 1123 K the tungsten carbide formation decreased the thermal conductivity of the materials. The maximum thermal diffusivity was $8x10^{-6}$ m^2/s with 66% density. This value was lower than the bulk tungsten but still higher than thermally sprayed tungsten that has lower porosity. Temperatures below 1273 K must be sued to maintain tungsten microdiamond composite by preventing excessive carbide formations. [19]

3. DISCUSSION AND CONCLUSION

In this paper, it was evaluated that the properties of the plasma facing components were highly dependent on the fabrication method and the material selection. As a result of the experiments within the literature, conclusions have been derived and discussed in this part.

Tungsten coatings over graphite could be done by direct current magnetron sputtering under 0.4 Pa - 0.6 Pa, 100 V bias voltage, 100 ºC substrate temperature, 200 mA discharge current, 300 V discharge voltage, and 4 cm working distance. The deposition rate was up to 8 nm/s. When the coating thickness reaches 2 μm, cohesive failure was observed. The mechanical properties of the film were improved by having a 0.4 ion to neutral flux ratio. The magnetron sputtered tungsten coatings over graphite substrate exhibits adhesion failure due to low argon pressure operation conditions which induce compressive stresses to the coating. The compressive residual stresses can be reduced by etching. However, adhesion failure still occurs at 11 MW/m^2 thermal loading. ***[14] [17]***.

The pulsed laser deposition technique successfully deposits tungsten (BCC) over amorphous fine grain graphite (hexagonal) with a strain of $2x10^{-3}$. The coating is uniform without any defects or visible cracks. The oxygen contamination is below 1%. Laser energy has an impact on the thickness of the tungsten coating by changing the crystalline size. The thicknesses from 120 nm to 300 nm were successfully deposited. Using 500 mJ laser energy exhibits the best characteristics for the coating ***[3]***.

The structure and the density of the tungsten coatings had a huge impact on their failure mechanisms, thermal behaviors, and critical loads. A higher temperature increase was observed during heat loading tests for the low-density inert plasma-sprayed tungsten coatings. The porous structure of the tungsten coating reduced the thermal conductivity and the mechanical strength thus lead to crack formations. However, the propagation of the formed cracks was delayed by a lamellar structure with a large pore structure that acted like a crack arrester and reduced thermal stresses during heat loading tests. In the case of high-density vacuum plasma sprayed coatings, higher thermal conductivity, and mechanical strength was observed. The presence of the homogeneously distributed small pores has increased the ductility of the coating. The mechanical strength of the vacuum sprayed tungsten coatings may reduce due to the presence of the unmolten particles that acted as stress concentration zones and delamination took place. Also, crack propagation was less controlled and went through the graphite substrate. The

physical vapor deposited tungsten coating has suffered a thermal expansion coefficient between the graphite and the tungsten coating that prompted by columnar grain structure. The diffusion barrier was found to be useful to prevent carbide formation within the layer. In the case of a rhenium diffusion barrier, the thermal properties of the tungsten coating did not affect significantly due to the thermal expansion coefficient differences of the tungsten and rhenium. If the thickness of the coating is thick enough to slow down the carbon diffusion through the whole coating, the carbide thin film formation at the interface during the annealing process also acts as a diffusion barrier, especially in cyclic loadings. The operation conditions and the growth rate of the carbides are determining factors for the minimum coating thickness. In the case of physical vapor deposited coating, this minimum thickness was found to be between 30 μm and 100 μm. Besides, the heat flux tests of the coatings prove that plasma sprayed tungsten coatings with a diffusion barrier exhibits the best performance for divertor applications[12] [4].

The high-temperature loads lead to carbide formations inside the tungsten and molybdenum interlayered coatings on the carbon-based substrates. The SEM and TEM analysis have demonstrated that annealed molybdenum layers will completely transform to the carbide and inside the tungsten layer, both W_2C and WC formation occurred within an hour. As the annealing time increases the carbide thickness also increased. The surface morphology also affected the carbon diffusion to the coating. Besides, the mechanical properties of the coatings decrease due to the brittle carbide phase presence. The failure load that leads to crack formation within the coating decreases as the annealing time increase. More precise results can be obtained if different annealing temperatures are considered for the carbide formation mechanism [1].

In the case of the tungsten coatings and carbon-based substrate, the strength of the tungsten coating is directly related to the adhesion strength. The chemical vapor deposited tungsten coatings exhibit the lowest residual stresses (200MPa) with respect to the fiber orientation. The physical vapor deposited tungsten coatings display stress states above 800 Mpa. During the low cycle fatigue tests, only physical vapor deposited tungsten coating with a molybdenum interlayer survived. The others exhibit cracking and buckling. Switching to edge localization mode this coating also exhibits delamination (lateral failure) on several spots. As a result, thin coatings are not advised to be used in JETs. Even by reducing the power density of the load by two orders of magnitude the failure cannot prevent. However, the thick plasma sprayed coatings withstand 23.5 MW/m^2 screening load and up to 10.5 MW/m^2 cyclic load. The high porosity within the thick coatings also helps to reduce the stresses and delay the failure. Besides, some

of the vacuum plasma sprayed coatings can withstand edge localized mode up to 0.35 GW/m^2. Carbon fiber composite substrates develop local delamination due to low tensile strength and fiber orientation dependence. The graphite has a thermal expansion coefficient which is closer to the tungsten. Using graphite over carbon fiber composite reduces the risk of delamination. In conclusion, chemical vapor deposition is a promising technique to fabricate tungsten coatings for fusion application. The coatings exhibit great stability at high temperatures, good thermal conductivity and, pure structure. Also, the coatings display resistance to deuterium blisters and retention is better than bulk tungsten. Some of the future requirements of the chemical vapor deposited tungsten coatings are; achieving a thick coating, testing on fusion relevant conditions and the industrial-scale fabrication methods must be evaluated by reducing high residual stresses. Besides, the cost of chemical vapor deposited tungsten coating is very high compared to plasma sprayed tungsten coatings [11] [21].

REFERENCES

- *Carbide formation in tungsten coatings on carbon-fibre reinforced carbon substrates. Thin Solid Films. 531. 21-25. Rasinski, Marcin & Maier, H. & Ruset, Cristian & Lewandowska, M. & Kurzydłowski, K.J. (2013)* [1]

- *Evaluation of nanosecond laser ablation and scratch resistance of tantalum carbide coated graphite substrates. Ceramics International Volume 45, Issue 17, Part B Pages 22578-22588 DVN Harish, Bharatish A, HN Narasimha Murthy, B. Anand, L. Rangaraj (2019)* [2]

- *The properties of the tungsten coating on fine grain graphite using pulsed laser deposition. Fusion Engineering and Design Volume 148 G.Antar, J.Alib, C.Madia, M.Nounc, V.Rohded, M.Roumiéc, A.J.Saidb, J.Younesa (2019)* [3]

- *High-Heat-Flux Loading of Tungsten Coatings on Graphite Deposited by Plasma Spray and Physical Vapor Deposition, Fusion Technology, 32:2, 263-276, C. García-Rosales, S. Deschka, W. Hohenauer, R. Duwe, E. Gauthier, J. Linke, M. Lochter, Werner K. W. M. Malléner, L. Plöchl, P. Rödhammer, A. Salito & Asdex-Upgrade Team (1997)* [4]

- *Thermal Analysis of Tantalum Carbide-Hafnium Carbide Solid Solutions from Room Temperature to 1400 °C. Zhang, C., Loganathan, A., Boesl, B., & Agarwal, A. (2017).* [5]

- *A Molybdenum Carbide / Carbon Composite and Manufacturing Method A. Bertarelli, S. Bizarro (2013).* [6]

- *The high temperature interaction between Molybdenum and Graphite Journal of Materials Science, Volume 10, Number 11, Page 1976 R. B. Matthews, G. M. Jenkins (1975)* [7]

- *Adhesion of advanced overlay coatings: mechanisms and quantitative assessment. Surface and Coatings Technology. Volume 71, Issue2, 201-207 H. Weiss (1995)* [8]

- *X-ray diffraction determination of texture and internal stresses in magnetron PVD molybdenum thin films. Surface and Coatings Technology, Volume 50, Issue 1 Zaouali J., L. Lebrun, P. Gergaud (1991)* [9]

- *Thermal Performance of Multilayer PVD Tungsten Coating for the First Wall Application in Nuclear Fusion Devices, Fusion Science and Technology, 68:2, H. Kim, Ho Jung Lee & C. Jang (2015)* [10]

- *Investigation of tungsten coatings on Graphite and CFC R. Neu1, H. Maier, E. Gauthier, H. Greuner1, T. Hirai, Ch. Hopf, J. Likonen, G. Maddaluno, G. F. Matthews, R. Mitteau (2007)* [11]

- *Manufacturing and high heat flux loading of tungsten coatings on fine grain graphite for the ASDEX-upgrade divertor S.Deschka, C.García-Rosalesa, W.Hohenauerb, R.Duweb, E.Gauthierc, J.Linkeb, M.Lochterd, W.Mallénerb, L.Plöchle, P.Rödhammerc, A.Salitof Journal of Nuclear Materials (1996)* [12]

- *Development of W Coatings for Fusion Applications. Fusion Engineering and Design Ruset, Cristian & Grigore, E. & Maier, H. & Neu, R. & Greuner, H. & Mayer, Matej & Matthews, G. (2011)*[13]

- *Properties of tungsten coatings deposited onto fine grain graphite by different methods. Surface and Coatings Technology. 142-144. Maier, H. & Luthin, J. & Balden, M. & Linke, Jochen & Koch, F. & Bolt, H.. (2001)* [14]

- *The Influence of Interface Characteristics on the Adhesion/Cohesion of Plasma Sprayed Tungsten Coatings. Coatings. 3. 108-125. Matějíček, Jiří & Vilémová, Monika & Musalek, Radek & Sachr, Pavel & Hornik, Jakub. (2013)* [15]

- *Properties of Electrodeposited Tungsten Coatings on Graphite Substrates for Plasma Facing Components. Journal of Fusion Energy. Sun, Ningbo & Lang, Shaoting & Zhang, Yingchun & Xu, Yuping & Liu, Hui & Li, Guangbin. (2016)* [16]

- *Magnetron-Sputter Deposition of W Coatings for Fusion Applications. Medziagotyra. 15. Pranevicius, L. (2009)* [17]

- *ITER Plasma Facing Components Magnetron-Sputter Deposition ITER Documentation Series, No.30 (1991)* [18]

- *Tungsten–microdiamond composites for plasma facing components V.Livramentoa, D. Nunesa, J.B. Correiaac, P.A. Carvalhoab, U. Mardolcarb, R. Mateusa, K. Hanadad, N. Shohojic, H. Fernandesa, C. Silvaa, E. Alvese (2011)* [19]

- *Properties of tungsten coatings deposited onto fine grain graphite by different methods. Maier, H. & Luthin, J. & Balden, M. & Linke, Jochen & Koch, F. & Bolt, H. (2001)* [20]
- *Recent research and development of thick CVD tungsten coatings for fusion application. Chen, Z., Lian, Y., Liu, X. (2020)* [21]
- *Manufacturing of tungsten and tungsten composites for fusion application via different routes. Wu, Y. (2019)* [22]
- *Thin-film deposition with physical vapor deposition and related Technologies. S.M. Rossnagel (2003)* [23]
- *Understanding plasma spraying. P. Fauchais (2004)* [24]
- *Introduction to Chemical Vapor Deposition (CVD) Creighton, J. (2001)* [25]